A Kinetic Model for Predicting Trace Gas Uptake and Reaction

Kevin R. Wilson,[1,*] Alexander M. Prophet,[1,2] and Megan D. Willis[3,*]

[1]*Chemical Sciences Division, Lawrence Berkeley National Laboratory, Berkeley, CA 94720*

[2]*Department of Chemistry, University of California, Berkeley, CA 94720*

[3] *Department of Chemistry, Colorado State University, Fort Collins, CO, USA*

Abstract

A model is developed to describe trace gas uptake and reaction with applications to aerosols and microdroplets. Gas uptake by the liquid is formulated as a coupled equilibria that links gas, surface and bulk regions of the droplet or solution. Previously, this framework was used in explicit stochastic reaction-diffusion simulations to predict the reactive uptake kinetics of ozone with droplets containing aqueous aconitic acid, maleic acid and sodium nitrite. Using prior data and simulation results, a new equation for the uptake coefficient is derived, which accounts for both surface and bulk reactions. Lambert *W* functions are used to obtain closed form solutions to the integrated rate laws for the multiphase kinetics; similar to previous expressions that describe Michaelis–Menten enzyme kinetics. Together these equations couple interface and bulk processes over a wide range of conditions and don't require many of the limiting assumptions needed to apply resistor model formulations to explain trace gas uptake and reaction.

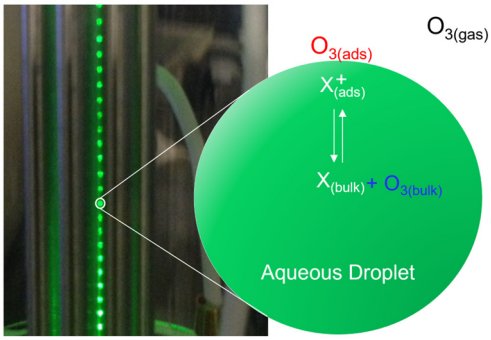

Correspondence to krwilson@lbl.gov and megan.willis@colostate.edu

I. Introduction

Multiphase and heterogeneous processes play significant roles within the complex network of gas phase reactions that control the composition of our atmosphere.[1-4] Reactions in and on cloud droplets and aerosols shuttle molecules between phases, acting both as reactive sources and sinks for atmospheric trace gases. Unlike purely gas phase reactions, multiphase reaction rates are often difficult to predict, in large part because of the substantial uncertainty in understanding how key non-reactive elementary steps govern the transfer and reaction of a gas molecule across an interface into the droplet or aerosol interior. These non-reactive steps, which include trace gas adsorption/desorption, solvation/de-solvation and diffusion introduce complex coupling and feedbacks that are absent for reactions occurring in a single phase.

The reactive uptake coefficient (γ) or reaction probability is the fraction of gas-surface collisions that yield a reaction. γ is perhaps the closest analog to a bimolecular rate constant in a homogeneous phase. However, despite the relative ease with which modern aerosol techniques are used to determine reaction probabilities, there remains a substantial challenge in connecting γ with a bimolecular reaction rate coefficient of a single elementary step.[5] This challenge arises because γ is an aggregate of many kinetic steps, leading to cases where the observed uptake coefficient and decay kinetics depend in complex ways on the gas, interface and condensed phase environment of the aerosol or droplet.[6] This complexity requires the development and application of models to interpret γ, with the goal of linking the physical properties of the aerosol or droplet with its multiphase reactivity.

There is a large number of published models and frameworks (see review by Kolb *et al.,*[7] and references therein) to describe gas uptake and reaction by aerosols and droplets. These models share the same basic elements required for connecting gas phase diffusion, interface

adsorption/desorption with solvation and diffusion in the bulk liquid.[8] However, many of these models differ in their starting assumptions and the subsequent approximations needed to achieve tractable solutions. Danckwerts[9, 10] derived equations for the coupling of diffusion and solubility, which serves as a basis for many subsequent approaches. Schwartz,[11] and later Shi and Seinfeld,[12] identified characteristic timescales for limiting cases where aqueous phase uptake by droplets is limited by either kinetics or mass transport. Hansen *et al.*[13] used a similar approach to describe stratospheric heterogeneous chemistry. Kinetic resistance models have been developed and refined by many authors.[2, 14-26] These formalisms approximate uptake as set of decoupled and normalized fluxes expressed as resistances, which can be added in series or in parallel in analogy to electrical circuits. Resistor models provide simple expressions for estimating uptake coefficients and in some cases the associated decay kinetics of the trace gas or solute. Analysis of experimental data by resistor models often requires assuming where the reaction occurs (surface vs. bulk), which as we will show in this work, is often not straightforward. Despite their widespread use, resistor model limiting cases may not accurately account for realistic multiphase reactions measured in the laboratory or that occur in the atmosphere.

To go beyond resistor-type models with simplified closed form expressions for limiting cases, a number of frameworks[19, 27-30] have been implemented in kinetic simulations to account for more complex multiphase chemistry. Smith *et al.*[22] examined the uptake and reaction of O_3 with oleic acid, comparing the resistor model with results obtained by numerically solving the coupled partial differential equations for diffusion and reaction. Kinetic multilayer models[31-38] employ a flux-based representation, numerically solving the coupled differential equations for mass transport and chemical reactions. Many multilayer models require a comprehensive set of variables for each molecule and so are often employed in inverse modeling studies[5, 39] of large data sets,

where they can resolve the fine details of surface and bulk processes as well as the formation of chemical gradients. Kinetic descriptions of multiphase chemistry, implemented in stochastic reaction-diffusion simulations by Houle,[40] Wilson[41] and coworkers,[6, 28, 42-47] have been used to describe multiphase transformations using a set of elementary kinetic and diffusion steps, with the goal of obtaining physically realistic, albeit simple descriptions, of reactive uptake. Despite the success of simulations in describing complex multiphase phenomena, there is a need for simple closed form expressions that go beyond limiting cases to accurately account for the coupling of surface and bulk processes needed to accurately predict trace gas uptake and reaction.

Here we derive a new set of equations for predicting reactive uptake and multiphase kinetics. The framework on which these derivations are based was recently implemented[48] in a stochastic reaction-diffusion simulation to explain the multiphase reaction rate of O_3 with aqueous droplets containing aconitic acid,[48] maleic acid[49] and nitrite.[50] The framework expresses the Henry's law constant as a product of two equilibria[17, 21, 26, 51] and explicitly includes diffusion and the coupling of surface and bulk processes, which are neglected in resistor-type models.

This paper is organized as follows. In Section II, we summarize the model framework and its assumptions, with a brief summary of how it was implemented in previous reaction-diffusion simulations.[48] In Section III prior simulation and experimental results are analyzed to derive an expression for γ and the associated closed-form kinetic equations, which include both surface and bulk reactions. In Section IV, we further test our model by comparing its predictions to previously published experimental results. Finally, in Section V, these predictions are extended to the dilute conditions relevant for the atmosphere.

II. Model Framework

The central elements of the model are shown in Fig. 1. A Henry's Law constant links the concentration of X in the gas phase with its liquid phase concentration (i.e. $[X_{(b)}]$) as illustrated in Fig. 1. Unlike other approaches that begin by connecting gas and liquid phase diffusional fluxes,

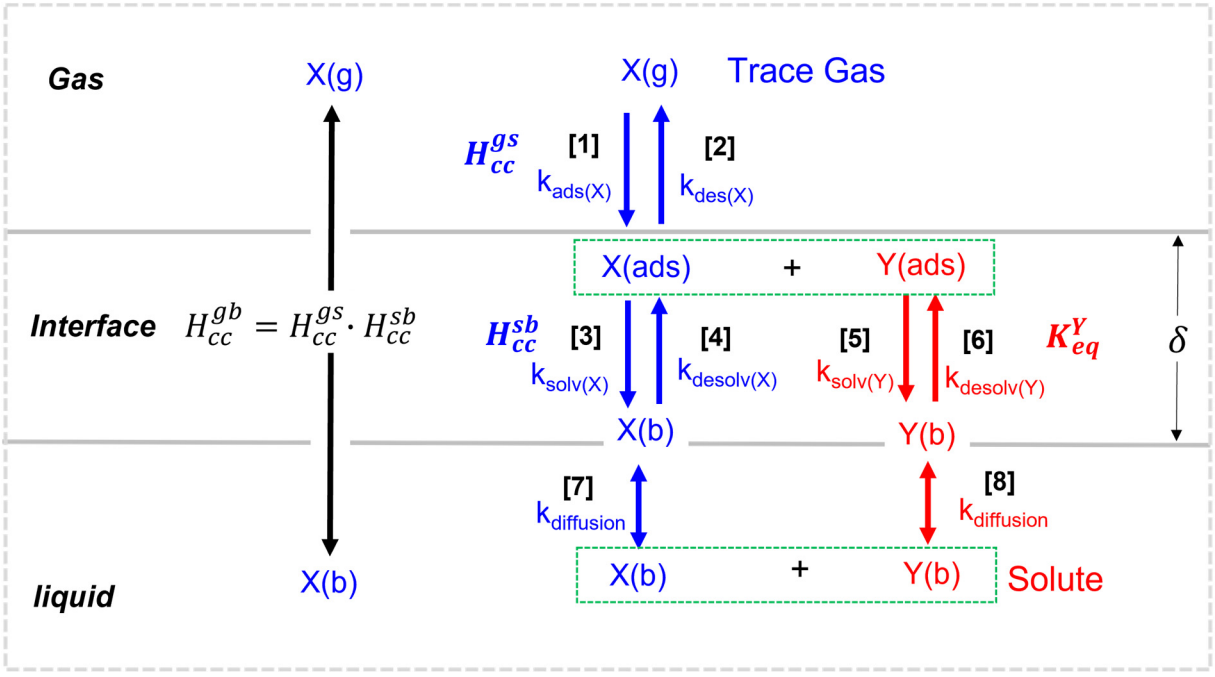

Figure 1: Model framework to describe the multiphase reaction of trace gas X (blue) with solute Y (red). The overall gas-to-bulk (gb) Henry's law constant is the product of two equilibria connecting gas (g), adsorbed (ads) and bulk (b) phase species. Each equilibrium is shown with its forward and backward elementary steps and rate constants. The green boxes show how the presence of a chemical reaction couples the equilibria of X and Y. δ is the thickness of the interface.

the overall Henry's law constant (H_{cc}^{gb}) for trace gas, $X_{(g)}$, is formulated as a product of two coupled equilibria; similar to previous expressions reported by Hansen,[17] Remorov and George.[21] For simplicity we use the dimensionless form of the Henry's Law constant, H_{cc}^{gb}. Thermodynamically, the Henry's law constant depends upon the difference in solvation free energy (ΔG_{sol}) between a molecule X in the gas phase (g) and in the bulk (b) liquid.

$$H_{cc}^{gb} = \exp\left(\frac{-\Delta G_{sol(gb)}}{RT}\right) \qquad \text{Eq. (1)}$$

$\Delta G_{sol(gb)}$ is negative for highly soluble gases and positive for those of low solubility. In reality, H_{cc}^{gb} is a product of two equilibria that describe the partitioning of X from the gas to the surface (gs) and the surface to the bulk (sb) as shown in Fig. 1,

$$H_{cc}^{gb} = H_{cc}^{gs} \cdot H_{cc}^{sb} \quad \text{Eq. (2)}$$

The magnitudes of H_{cc}^{gs} and H_{cc}^{sb} depend upon the difference in solvation energy for X in its gaseous state relative to its surface-adsorbed (ads) or bulk solvated states,

$$H_{cc}^{gs} = \exp\left(\frac{-\Delta G_{sol(gs)}}{RT}\right) \quad \text{Eq. (3)}$$

$$H_{cc}^{sb} = \exp\left(\frac{-\Delta G_{sol(sb)}}{RT}\right) \quad \text{Eq. (4)}$$

Although, H_{cc}^{gb} is a readily measurable quantity, the solvation energies required to compute H_{cc}^{gs} and H_{cc}^{sb} independently are not. Instead, $\Delta G_{sol(gs)}$ and $\Delta G_{sol(sb)}$ can be obtained in molecular dynamics (MD) simulations from the potential of mean force for transferring a molecule across an interface into the liquid.[52, 53] Although, $\Delta G_{sol(gb)}$ can either be negative or positive, simulations of the water surface for a range of different gases nearly always predict that $\Delta G_{sol(gs)}$ is negative.[52-56] This implies that aqueous interfaces are likely always enriched in X relative to the gas phase even for species such as N_2 and O_2.[52] Modeling studies that pre-date the wide-spread use of MD simulation typically assume $[X_{(g)}] = [X_{(ads)}]$.[8, 11] For O_3 the case is quite dramatic, with simulations[52-54, 57] indicating the O_3 is ~10 times enriched at the interface relative to the gas phase and ~300 times enriched at the surface relative to the bulk liquid.

As shown in Fig. 1, H_{cc}^{gs} and H_{cc}^{sb} can be expressed kinetically using the rate constants for forward and backward elementary steps,[48]

$$H_{cc}^{gs} = \frac{[X_{(ads)}]}{[X_{(g)}]} = \frac{(k_{ads(X)} \cdot \sigma) \cdot \Gamma_{\infty(X)}}{k_{des(X)} \cdot \delta} \quad \text{Eq. (5)}$$

$$H_{cc}^{sb} = \frac{[X_{(b)}]}{[X_{(ads)}]} = \frac{k_{solv(X)} \cdot \delta}{k_{desolv(X)} \cdot \Gamma_{\infty}} \quad \text{Eq. (6)}$$

where $\Gamma_{\infty(X)}$ is the maximum surface concentration (molec. cm^{-2}) of X and δ is the interface thickness. We assume an interfacial width of 1 nm, which is used to compute volumetric surface concentrations ($\frac{\Gamma_{\infty}}{\delta}$, molec. cm^{-3}). Table S1 summarizes the thermodynamic and kinetic relationships described by Eqs. (1-6).

As shown in Fig. 1 and Eq. (5), H_{cc}^{gs} is controlled by adsorption of $X_{(g)}$ to the surface (k_{ads}, step [1]) and its desorption from the interface back into the vapor (k_{des}, step [2]). As described in Willis and Wilson,[48] the elementary adsorption step [1] includes a sticking coefficient (σ), which is shown explicitly in Eq. (5). This quantity is more uncertain than other terms in the adsorption rate, such as the collision frequency and mean velocity of $X_{(g)}$.[48] σ is different from the mass accommodation coefficient (α) employed in other studies, which is a ratio of rate constants from two independent elementary kinetic steps (e.g. $\frac{k_{solv}}{k_{des}}$, steps [2] and [3]).[16]

H_{cc}^{sb} depends upon the solvation kinetics (k_{solv}, step [3]) of $X_{(ads)}$ into the bulk liquid and a desolvation step (k_{desolv}, step [4]), which brings $X_{(b)}$ to the interface. The kinetic steps of solvation and desolvation account for the enthalpic and entropic factors, beyond diffusion to/from the interface that occur when a solute (i.e., X or Y) transitions from the fully solvated liquid environment to the partially solvated, asymmetric environment of the interface. The critical cluster nucleation model[58] predicts a substantial barrier for solvation. In contrast, MD simulations[56, 59-63] indicate a negligible solvation barrier in most cases, suggesting that entropic factors maybe important. To our knowledge, there remains substantial uncertainty as to the correct molecular

picture of trace gas uptake (MD,[56, 60, 62, 63] critical cluster nucleation,[64] capillary wave[65]). Nevertheless, once solvated $X_{(b)}$, is free to diffuse (step [7], Fig. 1) throughout the liquid. For simplicity, surface diffusion is neglected. Elementary steps [1]-[4] are described and implemented in kinetic simulations[28, 48, 66] using a Langmuir framework, in which $X_{(g)}$ adsorbs and $X_{(b)}$ desolvates to specific sites at the interface, similar to the approach adopted by Remorov and Bardwell.[67]

Y is either a species dissolved in the liquid or the solvent itself (in the case of a purely organic aerosol that reacts with X). The partitioning of Y between the bulk and interface is governed by an equilibrium constant (K_{eq}^{Y}). Here we assume that Y is non-volatile and does not evaporate from solution. For cases where Y is volatile an additional equilibrium is needed and formulated in an analogous way as is described above for X. From Langmuir's equation[68] $[Y_{(ads)}]$ is,

$$[Y_{(ads)}] = \frac{\Gamma_{\infty(Y)}}{\delta} \cdot \frac{K_{eq}^{Y} \cdot [Y_{(b)}]}{1 + K_{eq}^{Y} \cdot [Y_{(b)}]} \qquad \text{Eq. (7)}$$

where,

$$K_{eq}^{Y} = \frac{k_{desolv(Y)}}{k_{solv(Y)}} \qquad \text{Eq. (8)}$$

$\Gamma_{\infty(Y)}$ is the maximum surface concentration of Y (in molec. cm^{-2}) and expressed as a volumetric concentration using δ. K_{eq}^{Y} is governed by two opposing elementary steps and is the ratio of rate constants for desolvation (step [6]) and solvation (step [5]) as is shown in Eq. (8). and schematically in Fig. 1.

The X + Y reaction occurs both within the bulk liquid and at its interface. At the surface, the reaction is assumed to proceed via a Langmuir-Hinshelwood mechanism (i.e. $X_{(ads)} + Y_{(ads)}$).

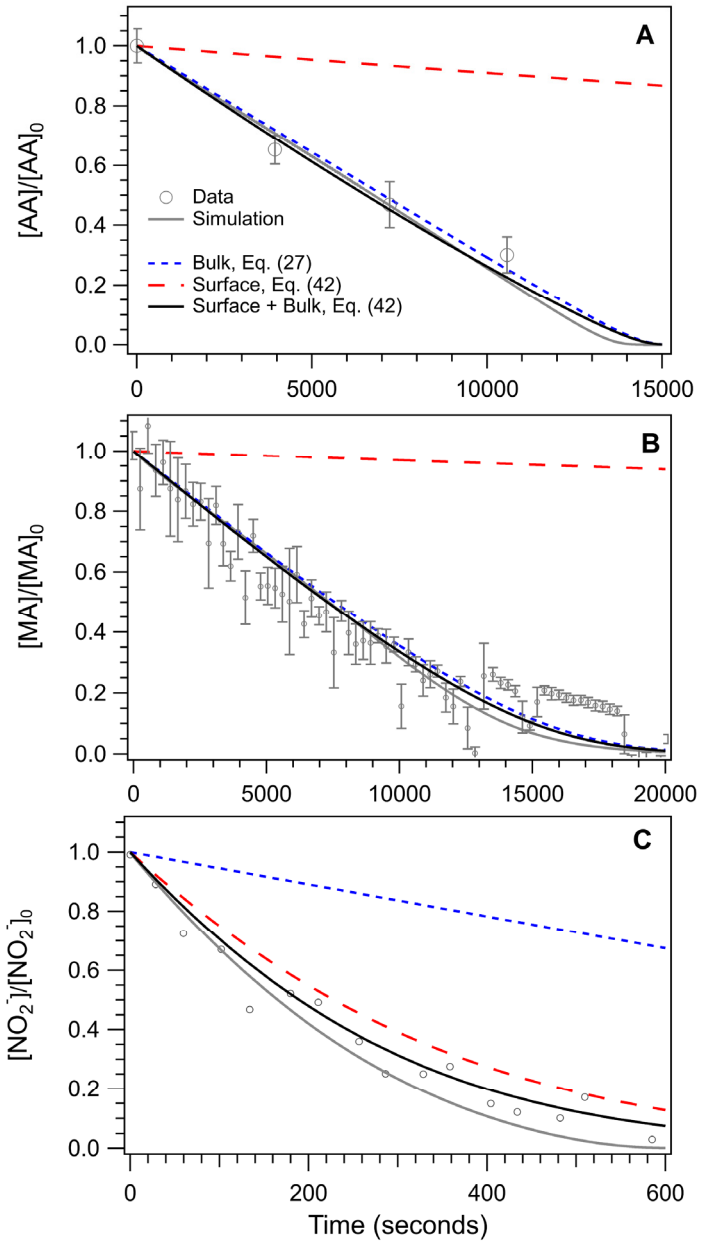

Figure 2 Normalized solute concentration vs. reaction time for: (A) aconitic acid, (B) maleic acid and (C) nitrite. The aconitic experimental conditions, from Willis and Wilson, are: r = 9.23 µm, $[AA]_0$ = 3.2 M, RH = 89.7% and $[O_{3(g)}]$ =58.4 ppm. Maleic acid experimental conditions (Dennis-Smither *et al.*) are: r = 4.59 µm, $[MA]_0$ = 7.4 M, RH = 63% and $[O_{3(g)}]$ = 38 ppm. The nitrite experimental conditions, from Hunt *et al.*, are: r = 5.75 µm, $[NO_2^-]_0$ = 0.2 M, RH = 86% and $[O_{3(g)}]$ = 12 ppm. Simulations are from Willis and Wilson. Bulk, surface and total (surface + bulk) kinetics are predicted using Eqs. (27) and (42).

As illustrated in Fig. 1 with green boxes, the reaction between X and Y dynamically couple three equilibria ($H_{cc}^{gs}, H_{cc}^{sb}, K_{eq}^{Y}$) as reactants are consumed and these three equilibria are forced to respond accordingly. This coupling, in addition to diffusion, produce complex feedbacks since the kinetic steps that comprise in these equilibria have characteristic response times to the perturbation of a chemical reaction.

The framework shown in Fig. 1, and described above, was previously implemented[48] in explicit stochastic reaction-diffusion simulations of the ozonolysis ($X_{(g)}$ = $O_{3(g)}$) of aqueous droplets. The simulation used two compartments to represent the two kinetically distinct regions of the droplet (i.e., gas/surface and surface/bulk shown in Fig. 1). Our framework is intended to be simple, so it does not resolve the formation of chemical gradients that might emerge, but instead considers [X] and [Y] as averaged quantities. Using literature validated O_3 solvation energies, rate coefficients, Langmuir and diffusion constants, our simulations[48] were able to predict the multiphase reaction kinetics of ozone with aqueous droplets containing *trans*-aconitic acid (AA), maleic acid[49] (MA) and nitrite[50] (NO_2^-) solutes. A comparison of the simulation results with experimental observations are replicated in Fig. 2. Key rate coefficients for O_3 that were used in the simulations are shown in Table S2. A full description of the simulation methods, reaction schemes, rate and diffusion coefficients and the comparison of the simulation results to the complete experimental data sets for AA (5 multi-droplet experiments), MA (6 single droplets), and NO_2^- (9 single droplets) can be found in Willis and Wilson.[48]

Here we build on our previous work to derive new expressions for the reactive uptake coefficient as well as closed form expressions for predicting the kinetics of trace gas uptake and reaction. These equations appear to be widely applicable to reactions occurring at aqueous surfaces, droplets and aerosols. We test these equations by comparing to an expanded data set,

which includes previously published ozonolysis studies of aqueous droplets containing ascorbic acid[69] and fumarate.[70]

III. Derivation

For the ozonolysis of AA and MA, event analysis revealed[48] that the reaction occurs mainly within the bulk liquid of the aerosol, in contrast with nitrite where the reaction is dominated by events at the surface. In Section IIIA, we first consider the case where ozonolysis only occurs in the bulk liquid, followed by Section IIIB where derivations are expanded to incorporate surface reactions.

IIIA. Bulk Reaction:

Derivation for Bulk Reactions: Neglecting surface reactions, the decay of Y (a solute in the droplet) is related to the reactive uptake coefficient (γ) by,[16]

$$\frac{d[Y]}{dt} = -\frac{3[X_{(g)}]\cdot\bar{c}\cdot\gamma}{4\cdot r} = -k_{b\_rxn}\cdot[X_{(b)}]\cdot[Y_{(b)}] \qquad \text{Eq. (9)}$$

where $\bar{c}$ is the mean speed of $X_{(g)}$, r is the droplet radius and k_{b_rxn} is the bimolecular rate coefficient for the X + Y reaction. To compute γ and to solve Eq. (9) for the time dependence of Y, requires deeper insight into the factors that control $[X_{(b)}]$. The following derivation and accompanying discussion is made more concrete by using an example reaction taken from our prior work[48] on the ozonolysis of *trans*-aconitic acid, where X = O_3 and Y = AA.

A characteristic feature of the O_3 + AA reaction,[48] is the depletion of bulk ozone inside the droplet relative to its Henry's Law steady state concentration in the absence of a reaction (i.e., $H_{cc}^{gb} \cdot [O_{3(g)}]$). This is shown in Fig. 3 where the average simulated $[O_{3(b)}]$ at early reaction times

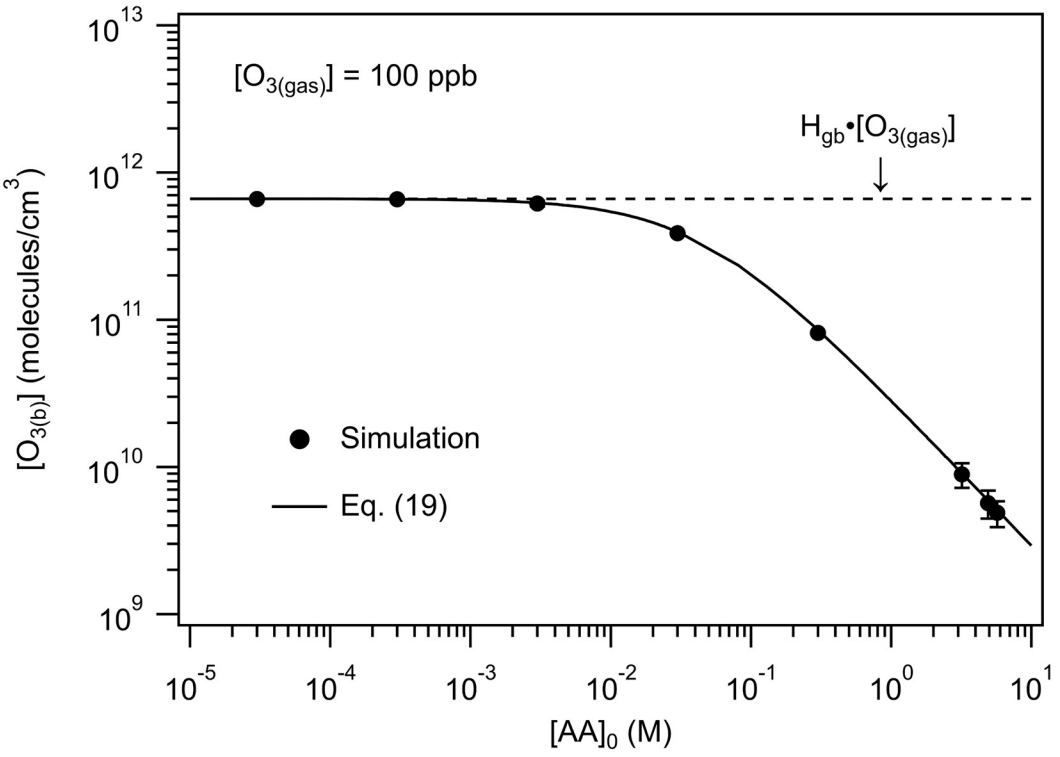

Figure 3: Simulated $[O_{3(b)}]$ vs. $[AA]_0$ at early reaction times (< 6 ms). Predictions from Eq. (19). Simulations and predictions are for a droplet r_0 = 9.1 μm. The dashed line shows the expected Henry's Law concentration of ozone in the droplet given a $[O_{3gas}]$ = 100 ppb. Details of the simulations can be found in Willis and Wilson.

is plotted vs. initial AA concentration ($[AA]_0$) in the droplet. When $[AA]_0$ is dilute (< 10^{-3} M), $[O_{3(b)}]$ resides at or near its Henry's law value. At larger $[AA]_0$, $[O_{3(b)}]$ increasingly deviates from its Henry's Law value and becomes ~100X depleted at $[AA]_0$ = 3 M. A quantitative description of O_3 depletion is essential for using Eq. (9) to reliably predict the decay kinetics of AA as well as to compute γ for this system.

The $[AA]_0$ where $[O_{3(b)}]$ becomes substantially depleted is ~3 x 10^{-2} M (30 mM) and corresponds to a pseudo first order loss rate (i.e., $k_{b\_rxn}\cdot[AA]_0$) of AA to O_3 of 253 s^{-1}. k_{b_rxn} for AA can be found in Table S3 with accompanying references. When $[AA]_0$ is > 30 mM the reaction consumes O_3 more rapidly than it can be replenished from the gas phase. In other words, $k_{b\_rxn}\cdot[AA]_0 > k_{transport}$, where $k_{transport}$ reflects the combined timescales for diffusive and kinetic transfer of O_3 into the droplet, as will be shown below.

The characteristic timescale for liquid phase diffusion is computed using the Einstein-Smoluchowski equation,[71, 72]

$$\tau_{diffusion} \approx \frac{L^2}{2\cdot D} \quad where\ L = \frac{r}{3} \qquad \text{Eq. (10)}$$

where L is distance and D the diffusion constant for O_3 in water (see Table S3). In prior simulations,[48] $L = \frac{r}{3}$ (i.e., the height of the simulated prism geometry) yielded an average timescale for O_3 diffusion into a 9.1 radius droplet of 2.6 ms. This corresponds to a rate coefficient for diffusion of 382 s^{-1} (i.e., $k_{diffusion} = \tau_{diffusion}^{-1}$); a value on the order of the reactive loss rate of O_3 at $[AA]_0$ ~3 x 10^{-2} M (253 s^{-1}). This shows that the depletion observed in Fig. 3 occurs when the chemical loss of O_3 occurs more rapidly than it can be replenished by transport from the gas phase.

In addition to diffusion, the transport rate of O_3 is, in some cases, also controlled by the kinetics of ozone solvation, desolvation, adsorption and desorption at the interface (steps [1]-[4] in Fig 1). We conducted a series of simulations to better understand how $k_{transport}$ scales with droplet size, as shown in Fig. 4. To obtain these O_3 transport timescales, simulations are run without reaction, using the same parameters for O_3 reported in Willis and Wilson[48] and shown in Table S2. Simulations are initialized with ozone only in the gas phase. The simulation output, which consists of the kinetic rise of $[O_{3(b)}]$ vs. time, is then fit to a $1 - e^{-k\cdot t}$ function to obtain $k_{transport}$. For all

sizes the time dependence of [$O_{3(b)}$] is well-represented by an exponential function as illustrated in Fig. S1. For large droplet sizes (r > 1 micron) in Fig. 4, $k_{transport} \approx k_{diffusion}$ where,

$$k_{diffusion} = \tau_{diffusion}^{-1} = \frac{2 \cdot D}{L^2} \qquad \text{Eq. (11)}$$

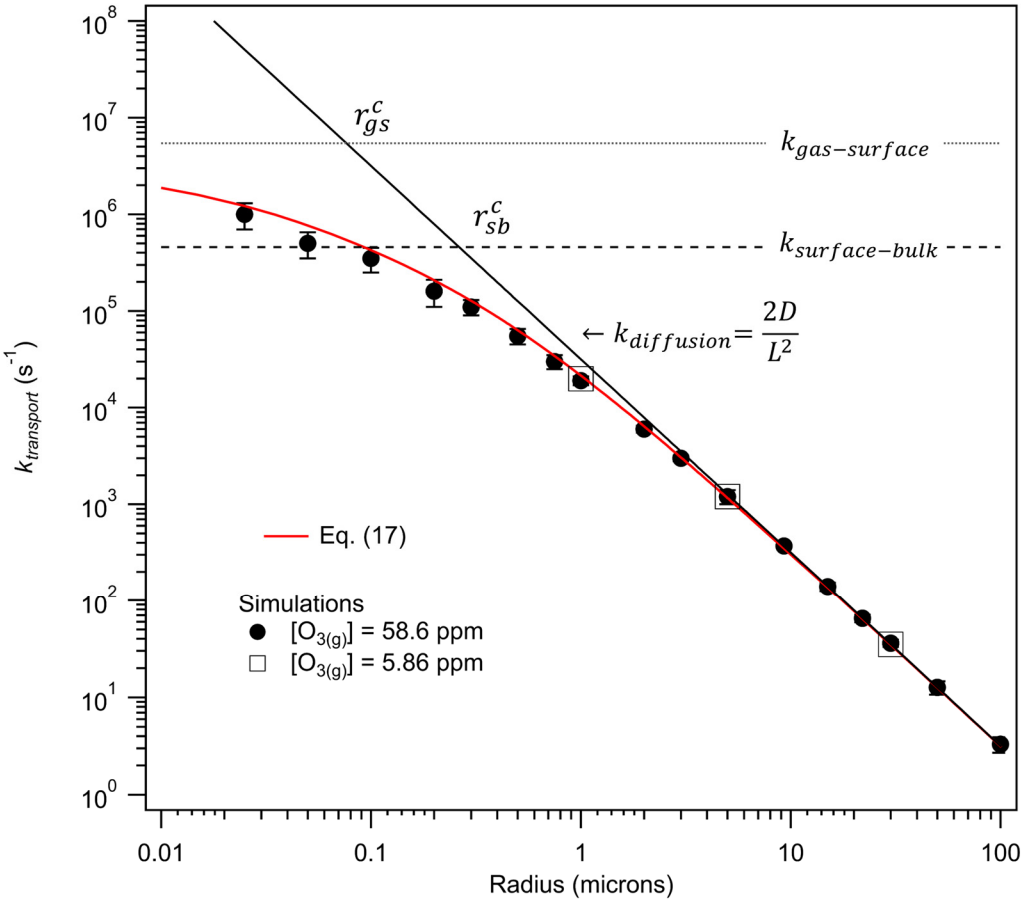

Figure 4: $k_{transport}$ vs. particle radius. Points are obtained from exponential fits to simulation results shown in Fig. S1. Error bars represent fitting errors of the simulation results. Lines show limiting cases where $k_{transport}$ is governed by diffusion and the kinetic steps of O_3 desorption and solvation. Also shown is a line computed using Eq. (17).

As the droplet size decreases, $k_{transport}$ increasingly deviates from $k_{diffusion}$ (i.e., $k_{transport} < k_{diffusion}$). This can be explained by the increasing importance of the additional kinetic timescales that compete with purely diffusive transport. These timescales, at the length scales considered here, do

not depend upon particle size, unlike $k_{diffusion}$. Within a Langmuir framework the characteristic kinetic timescale[73] for surface-to-bulk (sb, $k_{surface-bulk}$) transfer of $O_{3(ads)}$ is,

$$\tau_{surface-bulk}^{-1} = k_{surface-bulk} = k_{desolv} \cdot H_{cc}^{gb} \cdot \left[O_{3(gas)}\right] + k_{solv} \quad \text{Eq. (12)}$$

while the characteristic kinetic timescale for ozone to be transferred from the gas to the surface (gs, $k_{gas-surface}$) is,

$$\tau_{gas-surface}^{-1} = k_{gas-surface} = k_{ads} \cdot \sigma \cdot \left[O_{3(gas)}\right] + k_{des} \quad \text{Eq. (13)}$$

Using values for k_{ads}, k_{des}, k_{solv} and k_{desolv} from Ref. [48] and shown in Table S2, $k_{surface-bulk}$= 4.6 x 10^5 s^{-1} and $k_{gas-surface}$= 5.4 x 10^6 s^{-1}. $k_{transport}$ only weakly depends on $[O_{3(g)}]$ since k_{solv} and k_{des} are both much larger than the $k_{desolv} \cdot H_{cc}^{gb} \cdot \left[O_{3(g)}\right]$ and $k_{ads} \cdot \sigma \cdot \left[O_{3(g)}\right]$ terms in Eqs. (12) and (13), respectively.

It the surfactant literature[74] it is common to identify a critical radius or length-scale to determine the mode of mass transfer of solutes to a liquid interface (i.e., kinetic vs. diffusive). Here we borrow this concept and identify a pair of critical radii, r_{sb}^c and r_{gs}^c. The critical radii, shown in Fig. 4, denote locations where the diffusion rate of O_3 intersects with the kinetic timescales for gas-surface and surface-bulk transfer. At r_{sb}^c, $k_{diffusion} = k_{surface-bulk}$, whereas at r_{gs}^c $k_{diffusion} = k_{gas-surface}$. For O_3, r_{sb}^c is 263 nm and r_{gs}^c is 76.3 nm. For r >> $r_{sb}^c or\ r_{gs}^c$ transport of O_3 into the droplet is controlled by diffusion. As r approaches $r_{sb}^c or\ r_{gs}^c$ transport is more complex, exhibiting both kinetic and diffusive contributions. Although mass transport has been studied extensively using the concept of a single critical radius for the bulk-to-surface transport of surfactants in droplets and bubbles,[74] to our knowledge a solution to the dual critical radius problem has not been reported.

Without such a solution, we use approximate expressions to account for the size dependent behavior of $k_{transport}$ observed in the simulations (Fig. 4). This corresponds to a pair of equations to describe transport that includes both diffusive and kinetic contributions,

$$\frac{1}{k_{trans\_SB}} = \frac{\bar{R}^{-1}}{k_{diffusion}} + \frac{(1-\bar{R})^{-1}}{k_{surface-bulk}} \quad \text{Eq. (14)}$$

$$\frac{1}{k_{trans\_GS}} = \frac{\bar{R}^{-1}}{k_{diffusion}} + \frac{(1-\bar{R})^{-1}}{k_{gas-surface}} \quad \text{Eq. (15)}$$

where,

$$\bar{R} = \frac{r}{r+r_{sb}^{c}+r_{gs}^{c}} \quad \text{Eq. (16)}$$

$\bar{R}$ is a weighting function. When r is large compared to the critical radii, $\bar{R} \rightarrow 1$ and $1-\bar{R} \rightarrow 0$, so that $k_{diffusion}$ dominates $k_{transport}$. At $r = r_{sb}^{c}$ or r_{gs}^{c}, the kinetic and diffusive contributions to $k_{transport}$ are equal. As shown in Fig. 4, an average of k_{trans_SB} and k_{trans_GS},

$$k_{transport} = \frac{k_{trans\_SB}+k_{trans\_GS}}{2} \quad \text{Eq. (17)}$$

replicates $k_{transport}$ over the broad range of sizes observed in the simulations. For large droplets (r > 1 micron) transport occurs mainly by diffusion, while at smaller sizes (r < 500 nm) the transfer of O_3 into the droplet is increasingly limited by the kinetics of desorption and solvation; kinetic steps that occur on gas and liquid sides of the interface.

Using the expression for $k_{transport}$ in Eq. (17), we formulate a general expression to describe the relationship between O_3 reaction and transport. At very early reaction times when $[AA_{(b)}]_t \approx [AA_{(b)}]_0$, $[O_{3(b)}]$ is at quasi-steady state[48] (i.e., $\frac{d[O_{3(b)}]}{dt} = 0$).

$$\frac{d[O_{3(b)}]}{dt} = k_{transport} \cdot H_{cc}^{sb} \cdot \left[O_{3_{(ads)}}\right] - k_{b\_rxn} \cdot \left[O_{3(b)}\right] \cdot \left[AA_{(b)}\right]_0 - k_{transport} \cdot \left[O_{3(b)}\right] = 0 \quad \text{Eq. (18)}$$

$k_{transport}$ in Eq. (18) accounts for the transfer of O_3 into and out of the interior of the particle, whose rate depends also on $[O_{3(ads)}]$ and $[O_{3(b)}]$. Rearranging Eq. (18) and solving for $[O_{3(b)}]$ yields,

$$\left[O_{3_{bulk}}\right] = \frac{k_{transport} \cdot H_{cc}^{gb} \cdot [O_{3(b)}]}{k_{b\_rxn} \cdot \left[AA_{(b)}\right]_0 + k_{transport}} \quad \text{Eq. (19)}$$

with the following substitutions,

$$\left[O_{3(ads)}\right] = H_{cc}^{gs} \cdot \left[O_{3(b)}\right] \quad \text{Eq. (20)}$$

$$H_{cc}^{gb} = H_{cc}^{gs} \cdot H_{cc}^{sb} \quad \text{Eq. (21)}$$

We plot Eq. (19) as a function of $[AA]_0$ in Fig. 3. The close correspondence of the explicit simulation results with Eq. (19) confirms that O_3 depletion in the droplet at early reaction times is quantitatively explained by the competition between reaction and transport of O_3. Although Eq. (19) was derived to explain $[O_{3(b)}]$ at early reaction times where $[AA]_t \approx [AA]_0$, we expect that the relationship articulated in Eq. (19) is general and holds throughout the course of the reaction provided that $[AA]_t$ is known.

Substituting the expression for $[O_{3(b)}]$ from Eq. (19) into Eq. (9) yields,

$$\frac{d[AA]}{dt} = -\frac{3[O_{3(g)}] \cdot \bar{c} \cdot \gamma}{4 \cdot r} = -k_{b\_rxn} \cdot \left[\frac{k_{transport} \cdot H_{cc}^{gb} \cdot [O_{3(g)}]}{k_{b\_rxn} \cdot \left[AA_{(b)}\right] + k_{transport}}\right] \cdot \left[AA_{(b)}\right] \quad \text{Eq. (22)}$$

which is solved for γ_b to yield,

$$\gamma_b = \frac{k_{b\_rxn} \cdot \left[AA_{(b)}\right] \cdot 4 \cdot r}{3 \cdot \bar{c}} \cdot \left[\frac{k_{tranport} \cdot H_{cc}^{gb}}{k_{b\_rxn} \cdot \left[AA_{(b)}\right] + k_{transport}}\right]. \quad \text{Eq. (23)}$$

Substituting the expression for γ_b in Eq. (23) into Eq. (9) to compute the time dependence of the $\left[AA_{total\_b}\right]_t$, assuming only bulk reactions,

$$\frac{d[AA_{total\_b}]}{dt} = -H_{cc}^{gb} \cdot [O_{3(g)}] \cdot k_{b\_rxn} \cdot [AA_{(b)}] \cdot \left[\frac{k_{transport}}{k_{b\_rxn} \cdot [AA_{(b)}] + k_{transport}}\right] \quad \text{Eq. (24)}$$

which we integrate,

$$\int_{[AA_{(b)}]_0}^{[AA_{(b)}]_t} \frac{(k_{b\_rxn} \cdot [AA_{(b)}] + k_{transport}) \cdot d[AA_{total\_b}]}{[AA_{(b)}]} = \int_0^t -H_{cc}^{gb} \cdot [O_{3(g)}] \cdot k_{b\_rxn} \cdot k_{transport} \cdot dt$$

Eq. (25)

to produce the following expression,

$$\frac{k_{b\_rxn} \cdot [AA_{(b)}]_t}{k_{tranport}} + \ln[AA_{(b)}]_t = \frac{k_{b\_rxn} \cdot [AA_{(b)}]_0}{k_{transport}} + \ln[AA_{(b)}]_0 - H_{cc}^{gb} \cdot [O_{3(g)}] \cdot k_{b\_rxn} \cdot t \quad \text{Eq. (26)}$$

Eq. (26) is of the type $x + ln\ (x) = y$, which can be solved for x using a Lambert W function ($\mathbf{W}\{x\}$). The Lambert W function,[75, 76] sometimes known as the omega function, has been used extensively for obtaining closed formed solutions needed for evaluating Michaelis-Menten enzyme kinetics, dynamics in continuous flow tank reactors, Lindemann-Christiansen-Hinshelwood unimolecular dissociation kinetics, pharmacokinetics, H-indices, epidemic dynamics, etc.[77-82] Solving Eq. (26) yields,

$$[AA_{(b)}]_t = \frac{k_{transport}}{k_{b\_rxn}} \cdot \boldsymbol{W}\left\{\frac{k_{b\_rxn} \cdot [AA_{(b)}]_0}{k_{transport}} \cdot exp\left(\frac{k_{b\_rxn} \cdot [AA_{(b)}]_0}{k_{transport}} - k_{b\_rxn} \cdot H_{cc}^{gb} \cdot [O_{3(g)}] \cdot t\right)\right\} \quad \text{Eq. (27)}$$

for the specific case of the AA + O_3 reaction. The general solution is,

$$[Y_{(b)}]_t = \frac{k_{transport}}{k_{b\_rxn}} \cdot \boldsymbol{W}\left\{\frac{k_{b\_rxn} \cdot [Y_{(b)}]_0}{k_{transport}} \cdot exp\left(\frac{k_{b\_rxn} \cdot [Y_{(b)}]_0}{k_{transport}} - k_{b\_rxn} \cdot H_{cc}^{gb} \cdot [X_{(g)}] \cdot t\right)\right\} \quad \text{Eq. (27a)}$$

The Lambert W function is easily computed using built-in algorithms in *Mathematica*[83] (i.e *ProductLog* function), MATLAB (*W* function) and Python (*lambertw* function). There are several published analytical approximations to the Lambert W functions that could also be used.[84, 85] The

time dependence of $[O_{3(b)}]_t$ can then be obtained by replacing $[AA_{(b)}]_0$ in Eq. (19) with $[AA_{(b)}]_t$ from Eq. (27),

$$\left[O_{3_{(b)}}\right]_t = \frac{k_{transport} \cdot H_{cc}^{gb} \cdot [O_{3(g)}]}{k_{b\_rxn} \cdot \left[AA_{(b)}\right]_t + k_{transport}} \qquad \text{Eq. (28)}$$

or more generally,

$$\left[X_{(b)}\right]_t = \frac{k_{transport} \cdot H_{cc}^{gb} \cdot [X_{(g)}]}{k_{b\_rxn} \cdot \left[Y_{(b)}\right]_t + k_{transport}} \qquad \text{Eq. (28b)}$$

Validation of the Derivation for Bulk Reactions: Using Eqs. (23), (27) and (28), γ_b, $[AA]_t$ and $[O_{3(b)}]_t$ can now be computed from a small number of physical quantities (*i.e.*, $[O_{3(gas)}]$, D_{O3}, H_{cc}^{gb}, and k_{b_rxn}). Importantly, these equations link the bimolecular rate coefficients (k_{b_rxn}) measured

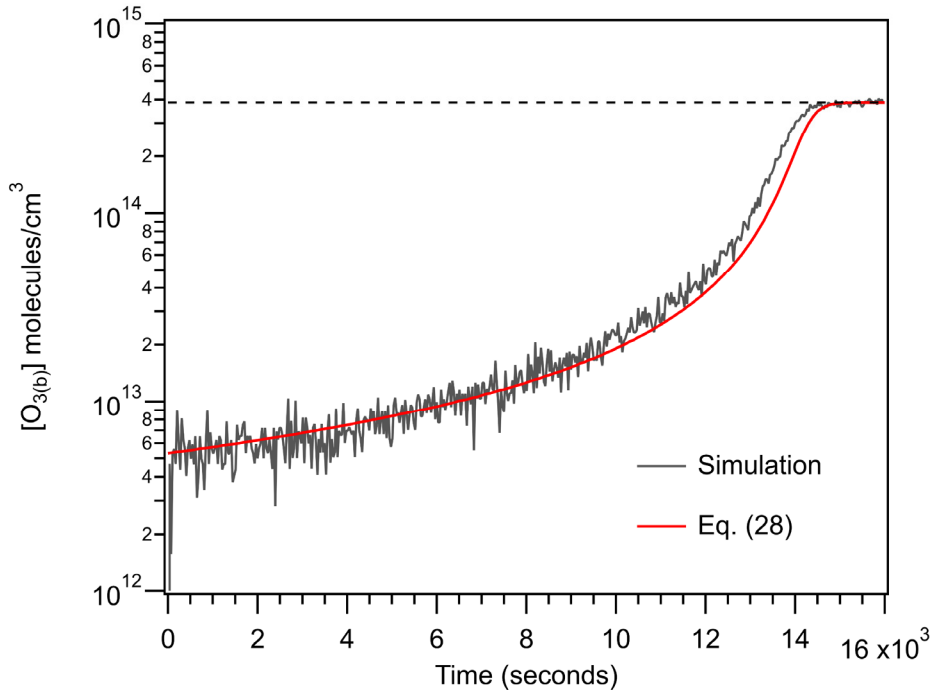

Figure 5: $[O_{3(b)}]$ vs. reaction time for an AA droplet. Experimental conditions (see Willis and Wilson): r = 9.23 µm, $[AA]_0$ = 3.2 M, RH = 89.7% and $[O_{3(g)}]$ =58.4 ppm. Explicit simulations from Willis and Wilson are compared with predictions from Eq. (28). Stochastic fluctuations are observed in the simulated $[O_{3(b)}]_t$. Dashed line indicates the Henry's law value for $[O_{3(b)}]$.

under dilute conditions in beaker-scale experiments to the reaction rate observed in microdroplets and submicron aerosols.

We use Eq. (27) to predict the decay kinetics of AA and MA shown in Figs. 2A and B. Rate coefficients are shown in Table S3. Eq. (27) is nearly indistinguishable from the explicit simulations[48] and replicates the experimentally measured decay kinetics of both MA[49] and AA.[48] This is not the case for NO_2^-, where the bulk predictions are too slow to accurately account for the measured and simulated multiphase kinetics (Fig. 2C). This is because surface reactions are significant as we have demonstrated with explicit simulations[48] and consider further in Section IIIB.

As an additional check, we compare the time dependence of $[O_{3(b)}]$ in the explicit simulations[48] with Eq. (28) for the experimental conditions of the AA droplet shown in Fig. 2A. As shown in Fig. 5, Eq. (28) predicts $[O_{3(b)}]$ as a function of reaction time and replicates the explicit simulations with some deviations near the end of the reaction as ozone approaches its Henry's law value.

We further compare the expression for γ in Eq. (23) with results from the explicit simulations for a fixed droplet size and variable $[AA]_0$ (r = 9.1 μm droplet with $[O_{3(gas)}]$ = 100 ppb). The simulated[48] kinetic decays of [AA] were used to compute an uptake coefficient using the following expression,

$$\gamma_{simulation} = \frac{4 \cdot \left(\frac{d[AA]}{dt}\right) \cdot r}{3 \cdot \bar{c} \cdot [O_{3(g)}]} \qquad \text{Eq. (29)}$$

The decay of [AA] vs. reaction time from the explicit simulations is nearly linear with time (i.e., zero order in [AA]) so we use the slope of the decay (i.e. $\frac{d[AA]}{dt}$) to compute $\gamma_{simulation}$. This

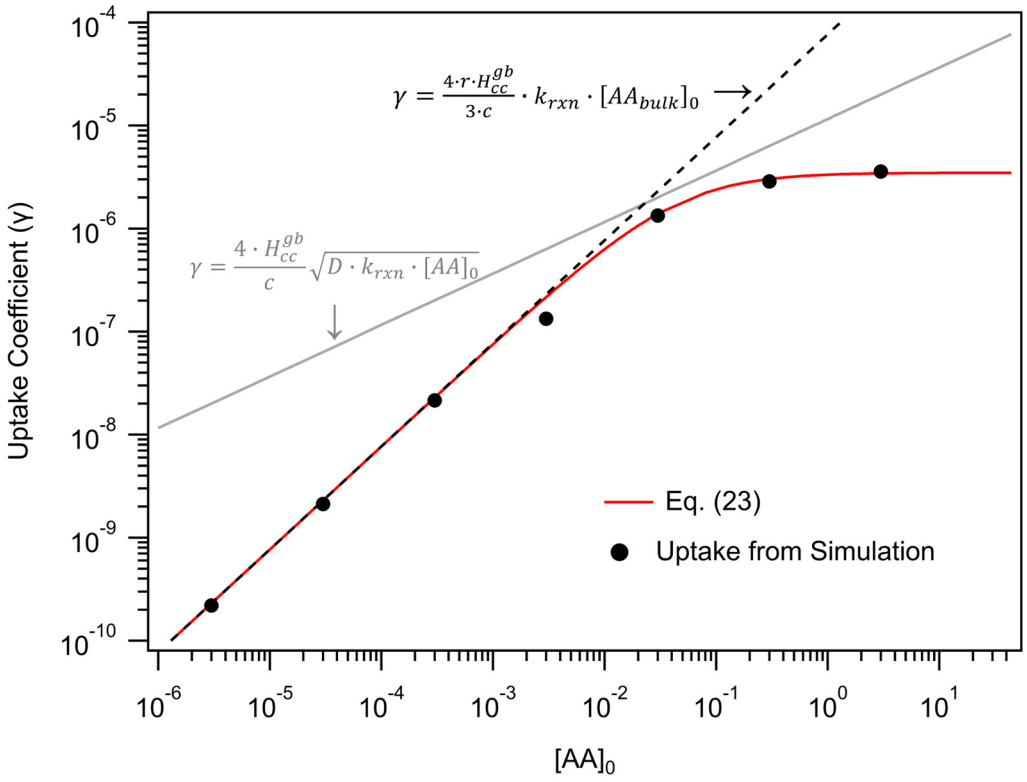

Figure 6: Reactive uptake coefficient (γ_b) vs. $[AA]_0$. Uptake coefficient from simulations compared with predictions from Eq. (23) and resistor model limiting cases (see Eqs. (30) and (31)). Simulations and predictions are for a droplet r_0 = 9.1 μm and $[O_{3gas}]$ = 100 ppb. Details of the simulations can be found in Willis and Wilson.

comparison is shown in Fig. 6 along with two expressions for γ from resistor model limiting cases.[16] Under dilute $[AA]_0$ conditions where reaction is much slower than transport, Eq. (23) reduces to,

$$\gamma_b \approx \frac{4 \cdot r \cdot H_{cc}^{gb}}{3 \cdot \bar{c}} k_{b\_rxn} \cdot [AA_{(b)}] \qquad \text{Eq. (30)}$$

since, $k_{b\_rxn} \cdot [AA_{(b)}]_0 \ll k_{transport}$, so that $\left[\frac{k_{tranport} \cdot H_{cc}^{gb}}{k_{b\_rxn} \cdot [AA_{(b)}]_0 + k_{transport}}\right] \approx H_{cc}^{gb}$. This is the same expression as resistor case #3 in Worsnop *et al.*[16] and case #1a in Smith *et al.*[22] Eq. (30) describes the case where reaction is slow relative to O_3 transport so that $[O_{3(b)}]$ throughout the reaction is

sustained at its Henry's Law concentration (i.e., the dilute or "phase-mixed" limit described by Schwartz[11]).

At higher $[AA]_0$ ozone is depleted, and the magnitude of the uptake coefficient is smaller than is predicted by Eq. (30), since the overall reaction rate is now transport controlled, which for AA is mainly by diffusion. Notably, as shown in Fig. 6, the predictions of Eq. (23) differ significantly from Danckwerts,[10] resistor case #2 ("uptake controlled by a 'fast' reaction") in Worsnop *et al.*[16] and case #1b ("diffusion-limited", or "reaction near the surface of the particle") in Smith *et al.*,[22]

$$\gamma_{resistor} = \frac{4 \cdot H_{cc}^{gb}}{\bar{c}} \cdot \sqrt{D_{x(b)} \cdot k_{b\_rxn} \cdot \left[Y_{(b)}\right]} \qquad \text{Eq. (31)}$$

where $D_{x(b)}$ is the diffusion constant of X (i.e., O_3) in water. Although, Eq. (31) has been used in many prior studies to explain experimental uptake measurements under diffusion-controlled conditions, this expression does not account for the observations presented here and discussed in Ref. [48] Instead, Eq. (23) faithfully captures the full evolution of the reactive uptake coefficient over a broad range of concentrations and connects, in a single expression, reaction-limited and diffusion-limited regimes, which has not been possible with resistor limiting cases.

γ_b in Eq. (23) is a non-monotonic function of r, as shown in Fig. 7A. This behavior arises from the size dependent interplay of transport (i.e., diffusion) and reaction, with droplet radius appearing in two locations in Eq. (23). The first term, plotted on the left axis of Fig. 7B, leads to an increase in γ_b with r due to the increase in gas phase collision frequency (and therefore reaction rate) as particle size increases. The second term (right axis of Fig. 7B) is a sigmoidal function of r scaling as $1/r^2$ due to the $k_{transport}$ term. For small sizes, $k_{transport} >> k_{b\_rxn} \cdot [AA]_0$ so Eq. (23) reduces to Eq. (30) and γ_b is expected to increase with r and is only limited by the ozonolysis reaction rate.

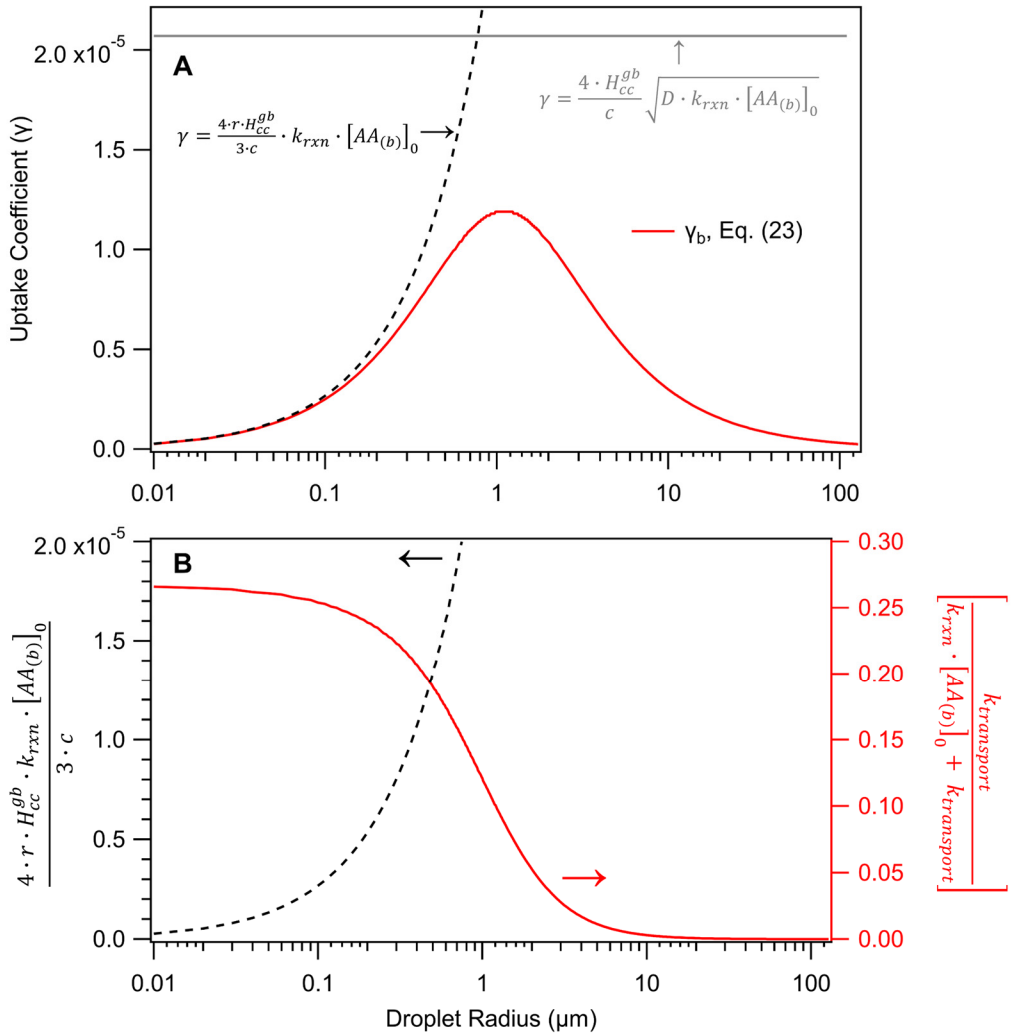

Figure 7: (A) Reactive uptake coefficient (γ_b) vs. droplet radius for $[AA]_0$ = 3.2 M. (B) The two terms in Eq. (23) that lead to the non-monotonic behavior of γ_b with radius shown in (A). Resistor model limiting cases are also shown (see Eqs. (30) and (31)).

As r continues to increase, the timescales for transport slow and approach those of the reaction so that the supply of O_3 to the droplet becomes limiting. This in turn slows the multiphase reaction rate, since average diffusion times increases with the square of distance (*i.e.,* radius). It is this size dependent shift in transport timescales relative to the reaction rates that controls the average $[O_{3(b)}]$ available in the droplet, which leads to the non-monotonic behavior of γ_b shown in Fig. 7A. The

shape and absolute magnitude of γ_b vs. r depends upon k_{b_rxn} and the solute concentration in the droplet. In contrast, Eq. (31) predicts that γ is independent of size.

The AA and MA experiments[48, 49] described above were conducted over a limited range of droplet sizes, so we are unable to experimentally validate the predicted non-monotonic behavior of γ_b in Eq. (23) and shown in Fig. 7. Thus, this prediction requires future experimental validation. New measurements are particularly important for sizes of around 1 micron. Unfortunately, this a challenging range for experiments to access, since it lies awkwardly between aerosol flow tube techniques for submicron particles and levitated droplet experiments that typically access r > 5 micron droplets. Nevertheless, predictions from Eq. (23) provide a seamless way of connecting multiphase reaction rates measured in super-micron droplets with those in submicron aerosols, while providing a means to link rate coefficients measured under dilute concentrations with concentrated aerosol and droplet conditions.

IIIB. Surface Reactions:

Derivation for Surface Reactions: The equations developed above only include bulk reactions. Expanding Eq. (9) to include surface contributions,

$$\frac{d[Y_{total}]}{dt} = -\frac{3[X_{(g)}]\cdot\bar{c}\cdot\gamma_{total}}{4\cdot r} = -k_{s\_rxn}\cdot[X_{(ads)}]\cdot[Y_{(ads)}] - k_{b\_rxn}\cdot[X_{(b)}]\cdot[Y_{(b)}] \qquad \text{Eq. (32)}$$

The total concentration of Y in the droplet ($[Y_{total}]$) now depends upon the reactive loss at both the interface and in the bulk. k_{s_rxn} and k_{b_rxn} are the surface and bulk rate coefficients, respectively. Without deeper experimental or theoretical insight into how surface rate coefficients might differ from their bulk analogs, we simply assume $k_{s\_rxn} = k_{b\_rxn}$. The $[Y_{(total)}]$ in the droplet can be expressed as a sum of two contributions (i.e., $Y_{(ads)}$ and $Y_{(b)}$),

$$[Y_{(total)}] = \frac{[Y_{(ads)}]\cdot V_s + [Y_{(b)}]\cdot V_b}{V_{total}} \quad \text{Eq. (33)}$$

where V_{total}, V_s and V_b are the total, surface and bulk volumes, respectively. For the droplets sizes considered here $V_b >> V_s$, so $V_{total} \approx V_b$. For a sphere,

$$\frac{V_s}{V_b} = \frac{r^3-(r-\delta)^3}{r^3} \quad \text{Eq. (34)}$$

where δ is the interface thickness. Substituting Eqs. (33) and (34) into Eq. (32) yields,

$$\frac{d[Y_{(total)}]}{dt} = -\frac{3[X]\cdot\bar{c}\cdot\gamma_{total}}{4\cdot r} = -k_{s\_rxn}\cdot[X_{(ads)}]\cdot[Y_{(ads)}]\cdot\left(\frac{r^3-(r-\delta)^3}{r^3}\right) - k_{b\_rxn}[X_{(b)}]\cdot[Y_{(b)}] \quad \text{Eq. (35)}$$

For a Langmuir-Hinshelwood reaction mechanism, $[Y_{ads}]$ is computed using Eqs. (7) and (8). Importantly, Eq. (35) assumes that throughout the reaction $[Y_{ads}]$ is solely controlled by the Langmuir equation (Eq. (7)). For very fast reactions, $[Y_{(ads)}]$ can be depleted when its diffusion rate and the kinetics of adsorption occur on timescales slower than its reactive loss. This case will be considered in a forthcoming publication where there is substantial depletion of interfacial iodide that occurs during multiphase ozonolysis.[86] Substituting $[Y_{(ads)}]$, $[X_{(b)}]$ and $[X_{(ads)}] = H_{cc}^{gs}\cdot[X_{(g)}]$ into Eq. (32) yields an expression for the total reactive uptake (γ_{total}) that now explicitly includes surface (γ_s) and bulk contributions (γ_b, Eq. (23)),

$$\gamma_{total} = \gamma_s + \gamma_b = \frac{4\cdot r\cdot[Y_{(b)}]}{3\cdot\bar{c}}\cdot\left(\left[\frac{k_{s\_rxn}\cdot H_{cc}^{gs}\cdot\Gamma_{\infty}^{Y}\cdot K_{eq}^{Y}}{1+K_{eq}^{Y}\cdot[Y_{(b)}]}\cdot\left(\frac{r^3-(r-\delta)^3}{r^3}\right)\right] + \left[\frac{k_{b\_rxn}\cdot k_{transport}\cdot H_{cc}^{gb}}{k_{rxn}[Y_{(b)}]+k_{transport}}\right]\right) \quad \text{Eq. (36)}$$

where,

$$\gamma_s = \frac{4\cdot r\cdot[Y_{(b)}]}{3\cdot\bar{c}}\cdot\left(\frac{k_{s\_rxn}\cdot H_{cc}^{gs}\cdot\Gamma_{\infty}^{Y}\cdot K_{eq}^{Y}}{1+K_{eq}^{Y}\cdot[Y_{(b)}]}\cdot\left(\frac{r^3-(r-\delta)^3}{r^3}\right)\right) \quad \text{Eq. (37)}$$

Unlike γ_b, γ_s does not have a size dependence due to the cancelation of r in the first term (RHS Eq. (37)) with the final V_s/V_b term. This is consistent, for example, with OH surface reactions on organic aerosols, which find that γ is independent of size.[24, 87]

To derive a closed form expression for the time dependence of $[Y_{(total)}]$ we start with the following expression,

$$\frac{d[Y_{(total)}]}{dt} = -k_{s\_rxn} \cdot \left[X_{(ads)}\right] \cdot \left[\frac{\Gamma_\infty^Y \cdot K_{eq}^Y \cdot [Y_{(b)}]_t}{1 + K_{eq}^Y [Y_{(b)}]_t} \left(\frac{r^3 - (r-\delta)^3}{r^3}\right)\right] - \left[Y_{(b)}\right]_t \qquad \text{Eq. (38)}$$

where previously we derived an expression for $[Y_{(b)}]_t$ in Eq. (27) in Section IIIA. Although the first term on the RHS of Eq. (38) depends upon $[Y_{(b)}]$ in order to compute $[Y_{(ads)}]$, the contribution of the surface reaction ($Y_{(ads)}$ + $X_{(ads)}$) to $\frac{d[Y_{(total)}]}{dt}$ is decoupled from the reaction occurring in the bulk droplet (i.e. $Y_{(b)}$ + $X_{(b)}$). This allows us to separately integrate the surface portion of Eq. (38),

$$\int_{[Y_{(b)}]_0}^{[Y_{(b)}]_t} \frac{(1 + K_{eq}^Y \cdot [Y_{(b)}])}{[Y_{(b)}]} \cdot d[Y_{(total)}] = \int_0^t -k_s \cdot \left[X_{(ads)}\right] \cdot \Gamma_\infty^Y \cdot K_{eq}^Y \cdot \left(\frac{r^3 - (r-\delta)^3}{r^3}\right) \cdot dt \qquad \text{Eq. (39)}$$

which yields,

$$K_{eq}^Y \cdot \left[Y_{(b)}\right]_t + ln\left(\left[Y_{(b)}\right]_t\right) = K_{eq}^Y \cdot \left[Y_{(b)}\right]_0 + ln\left(\left[Y_{(b)}\right]_0\right) - k_s \cdot \left[X_{(ads)}\right] \cdot \Gamma_\infty^Y \cdot K_{eq}^Y \cdot \left(\frac{r^3 - (r-\delta)^3}{r^3}\right) \cdot t \qquad \text{Eq. (40)}$$

For the ozonolysis reactions considered here, $[X_{(ads)}]$ is not depleted[48] due to the much slower speed of the surface reaction relative to ozone adsorption/desorption kinetics from the interface so that over the course of the reaction,

$$\left[X_{(ads)}\right] = H_{cc}^{gs} \cdot \left[X_{(g)}\right] \qquad \text{Eq. (41)}$$

Eq. (41) may not be applicable for very fast reactions at the interface that deplete [$X_{(ads)}$] (i.e., $[X_{(ads)}] < H_{cc}^{gs} \cdot [X_{(g)}]$). This case (i.e., O_{3ads} depletion) will be considered in some detail in a forthcoming publication on the mechanism of I^- + O_3 reaction in droplets.[86]

Eq. (40) is solved using the Lambert **W** function,

$$[Y_{(total)}]_t = \frac{1}{K_{eq}^Y} \cdot \boldsymbol{W}\left\{K_{eq}^Y \cdot [Y_{(b)}]_t \cdot exp\left(K_{eq}^Y \cdot [Y_{(b)}]_t - k_{s\_rxn} \cdot H_{cc}^{gs} \cdot [X_{(g)}] \cdot \Gamma_\infty^Y \cdot K_{eq}^Y \cdot \left(\frac{r^3-(r-\delta)^3}{r^3}\right) \cdot t\right)\right\} \quad \text{Eq. (42)}$$

where $[Y_{(b)}]_t$ was previously computed in Eq. (27a) and is,

$$[Y_{(b)}]_t = \frac{k_{transport}}{k_{b\_rxn}} \cdot \boldsymbol{W}\left\{\frac{k_{rxn} \cdot [Y_{(b)}]_0}{k_{transport}} \cdot exp\left(\frac{k_{rxn} \cdot [Y_{(b)}]_0}{k_{transport}} - k_{b\_rxn} \cdot H_{cc}^{gb} \cdot [X_{(g)}] \cdot t\right)\right\} \quad \text{Eq. (43)}$$

Eq. (42) includes contributions from both surface and bulk reactions. One can separately compute $[Y_{(total)}]_t$ for the cases where the reaction occurs only at the surface or in the bulk (Eq. 43) or the fully coupled case (Eq. (42)) where the reaction occurs in both locations. For example, substituting $[Y_{(b)}]_0$ into Eq. (42) instead of the expression for $[Y_{(b)}]_t$ in Eq. (43) eliminates the contribution from the bulk reaction, allowing one to see how much the surface reaction contributes to the kinetics of Y.

Validation of Derivation for Fully Coupled Reactions: Shown in Fig. 2 are predictions using Eq. (42) for the reaction of AA, MA, and NO_2^- with ozone. We compare the fully coupled (surface + bulk reaction) predictions with those predictions assuming the reaction either occurs entirely in the bulk or at the interface. The fully coupled prediction replicates the AA and MA data as well as the explicit simulations showing that surface reactions are minor, with the majority reaction occurring in the interior of the droplet. The surface-only predictions are a factor of 10-20 times too slow compared to the AA and MA experiments; this is not the case, however, for nitrite. The fully coupled predictions replicate the [NO_2^-] vs. reaction time observed in experiments by Hunt *et al.*[50]

as well as in the explicit simulations. Although surface reactions dominate for NO_2^-, the contribution of the bulk reaction is non-negligible (Fig. 2C), which is illustrated below by computing the surface and bulk contributions to the total uptake coefficient.

For nitrite, at the beginning of the reaction (i.e. $[NO_2^-]_t \approx [NO_2^-]_0$), event analysis from the explicit simulations reported in Willis and Wilson,[48] show that ~83% of the reactions occur at the interface. We use Eq. (36) to compute the overall uptake coefficient (γ_{total}) for the reaction, which is 3.04 x 10^{-5}. Using Eq. (37), the surface contribution to the total uptake coefficient is γ_s = 2.55 x 10^{-5}, whereas from the bulk reaction, γ_b = 4.88 x 10^{-6}. Thus, the surface fraction of the total uptake ($\gamma_{surface}/\ \gamma_{total}$) is 83.9%; in good agreement with the simulation event analysis. In contrast, the surface (i.e., γ_s/γ_{total}) contributes only 4.3% for MA and 11.6% for AA in these slower reacting and more-weakly surface-active systems.[48]

IV. Further Model Validation: Ozonolysis of Fumarate and Ascorbic Acid Droplets

We now use these equations to predict the ozonolysis kinetics of fumerate[70] (FA) and ascorbic acid[69] (AscA), previously reported in the literature, for which we have not performed explicit kinetic simulations. Predicting the multiphase kinetics of FA and AscA requires knowing the following quantities: k_{b_rxn}, Γ_∞, and K_{eq} in addition to the experimental conditions ($[O_{3(g)}]$, droplet size and initial solute concentration). Here we assume that $k_{b\_rxn} = k_{s\_rxn}$.

Shown in Fig. 8 are kinetic measurements reported by King *et al.*[70] for the ozonolysis of a droplet containing FA (r = 4-5 μm, $[FA]_0$ = 0.086 M, pH = 10, $[O_{3(g)}]$ = 1 ppm). Hoigne and Bader[88] reported a lower limit for O_3 + FA rate coefficient at pH 8 of k_{b_rxn} > 1 x 10^5 L mol^{-1} s^{-1}. Here we use k_{b_rxn} = 3 x 10^5 L mol^{-1} s^{-1}. It is likely that FA has a value of Γ_∞ that is similar to MA, as shown in Table S3. To our knowledge, K_{eq} for fumarate at pH = 10 has not be measured and is therefore

an adjusted parameter in Eq. (42). Using values of r = 4.5 μm, and K_{eq} = 5.6 x 10^{-21} cm^3 $molec.^{-1}$ (k_{solv} = 90 s^{-1}, k_{desolv} = 5.0 x 10^{-19} cm^3 $molec.^{-1}$ s^{-1}) yields a reasonable representation of the fumarate measurements reported by King *et al.*[70] in Fig. 8. The value of k_{desolv} is larger than used for MA, which was previously obtained using the relationships reported by Bleys and Joos.[73] This difference likely reflects differences in surface partitioning kinetics of neutral acids and their dianions. Nevertheless, given the experimental uncertainty, the predictions of Eq. (42) appear to capture the correct timescale and overall shape of the kinetic decay reported in Ref.[70] Importantly, the Lambert **W** function in Eq. (42) captures the observed exponential-like kinetics of FA (*i.e.,* first order in [FA]) and the more linear decay for diffusion limited bulk reactions that are zero order in AA and MA (Fig. 2). As can be seen in Fig. 8, the ozonolysis reactions occur mainly at

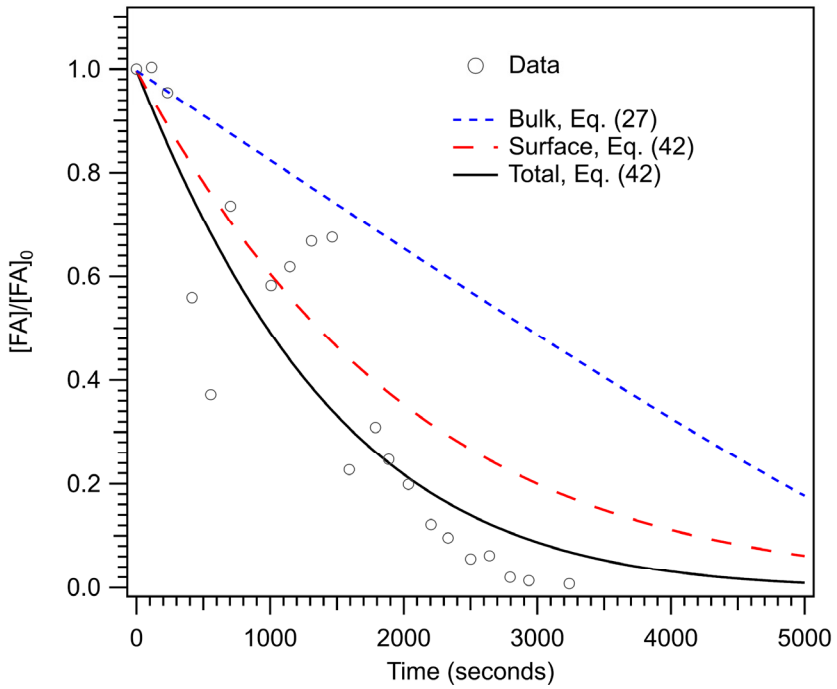

Figure 8: Normalized [FA] vs. reaction time. Data is from King *et al.* for r = 4.5μm, $[FA]_0$= 0.086 M, [O3(g)] = 1 ppm, and pH = 10. Bulk, surface and total (surface + bulk) kinetics are predicted using Eqs. (27) and (42). The kinetic decay of FA was quantified by King *et al.*, using Raman spectroscopy.

the surface, although the contribution from the bulk reaction is significant. At $[FA]_t \approx [FA]_0$, γ_s/γ_{total} is 73%, where $\gamma_{total} = 2.3 \times 10^{-5}$, $\gamma_s = 1.7 \times 10^{-5}$ and $\gamma_b = 6.1 \times 10^{-6}$.

Chang and coworkers,[69] reported an extensive study of the ozonolysis of ascorbic acid in aqueous microdroplets, using laser tweezers and Raman spectroscopy to quantify the multiphase kinetics. Shown in Table S4 are a set of 18 droplets measurements and the associated experimental conditions. This data set was collected at a pH 1.7-1.9 with ionic strengths between 0.5-1.5 M (NaCl). For the prediction we use the ozonolysis rate coefficient for ascorbic acid measured by Giamalva *et al.*[89] in bulk solutions ($k_{b\_rxn} = (6.9 \pm 2.3) \times 10^5$ L mol^{-1} s^{-1} at pH =2). This is reasonably

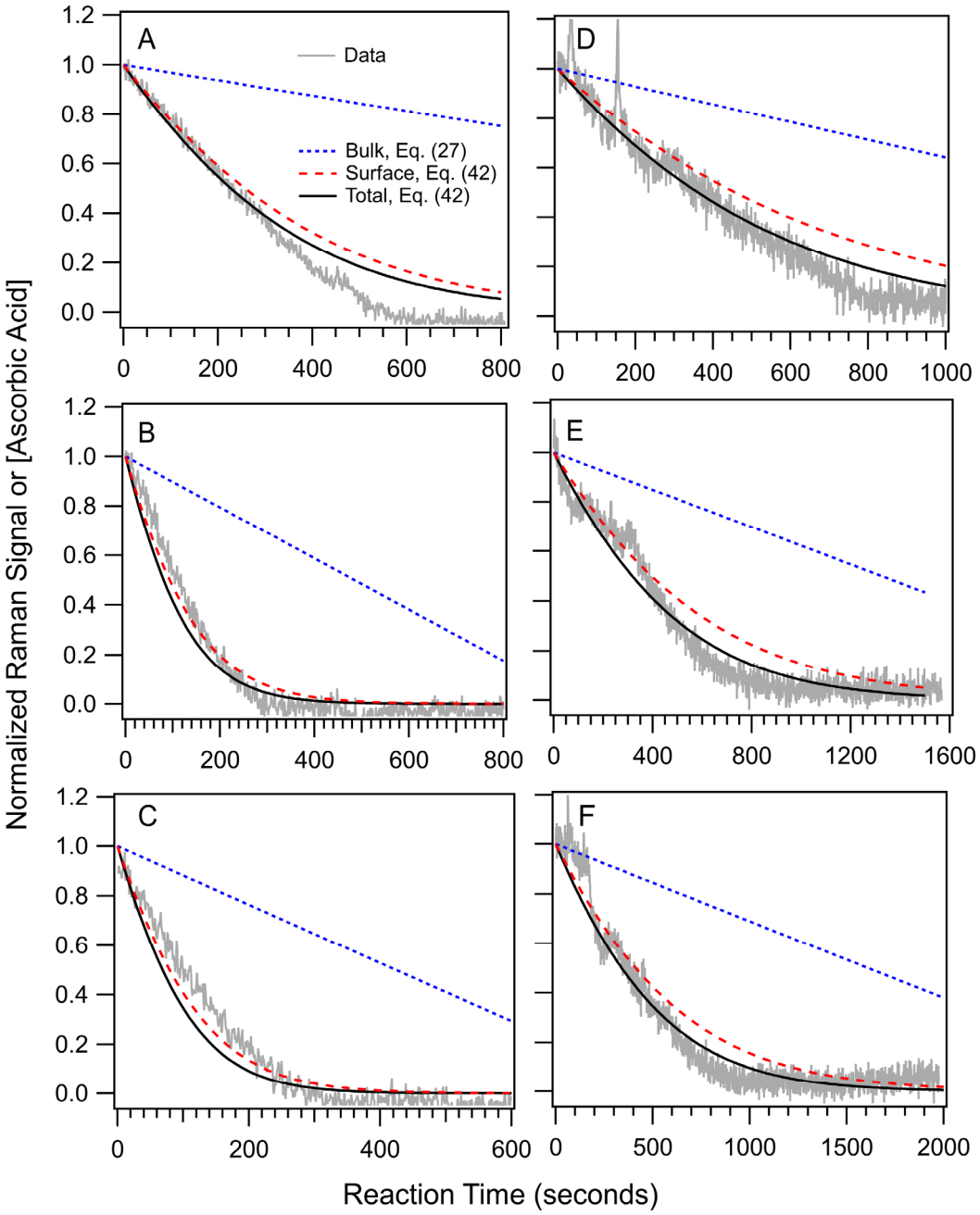

Figure 9: Normalized [AscA] vs. reaction time. The experimental data for the 6 droplet experiments (A-F) is from Chang *et al*. The reaction kinetics are monitored using Raman spectroscopy. The experimental conditions can be found in Table S4 and correspond to (A) expt. #1, (B) expt. #2, (C) expt. #3, (D) expt. #4, (E) expt. #5 and (F) expt. #6. Additional data for this systems is show in Figs. S2 and S3. Bulk, surface and total (surface + bulk) kinetics are predicted using Eqs. (27) and (42).

consistent with the value reported by Kanofsky and Sima[90] (k_{b_rxn} = 5.6 x 10^5 L mol^{-1} s^{-1}). We assume that Γ_∞ is the same as for MA and FA, as described above. We assume k_{solv} = 90 s^{-1} and

k_{desolv} = 2.5 x 10^{-20} cm^3 molec.$^{-1}$ s^{-1} to yield a value of K_{eq} = 2.8 x 10^{-22} cm^3 molec.$^{-1}$ These values are similar to those used by Willis and Wilson[48] for aconitic acid (a highly soluble tri-carboxylic acid), and are consistent with our intuition that ascorbic acid should be weakly surface active. Shown in Figs. 9, S3 and S4 are the predictions of Eq. (42) compared with the experimental measurements reported by Chang and coworkers.[69] Although, NaCl was added to the droplets, we have not corrected our Henry's Law constant for ionic strength, since we lack sufficient information for how the presence of ions alters the individual elements of the equilibria (i.e. H_{cc}^{gs} and H_{cc}^{sb}) that comprise H_{cc}^{gb}.

The agreement between our predictions and measurements is reasonable (Fig. (9)), especially at high experimental [$O_{3(g)}$]. For other droplets (see Figs. S2 and S3) the predictions deviate somewhat from observations, especially for some of the measurements conducted at [$O_{3(g)}$] = ~1-2 ppm, where the reaction timescales are much longer (> 2000 seconds). The origin of this discrepancy is unclear but may arise from neglecting ionic strength effects on the rate coefficient and Henry's law constant, or the presence of additional loss channels for ascorbic acid in the experiments, such as evaporation. Overall, the predictions suggest that for this system, the reaction occurs mainly at the surface (> 80%) with more minor contributions from reaction in the bulk droplet. To illustrate, γ_s/γ_{total} for droplet A is 89%, where γ_{total} = 7.2 x 10^{-5}, γ_s = 6.4 x 10^{-5} and γ_b = 8.1 x 10^{-6}.

Using five previous data sets[48-50, 69, 70] (AA, MA, nitrite, FA, and AscA) we have validated the model description presented here by showing that it can make reasonable predictions of the multiphase kinetics and uptake coefficients under both diffusionally and kinetically controlled conditions, using a single common framework. The model naturally accounts for the varying contributions of surface and bulk reactions enabling their relative contribution to be quantified.

Below we extend the model framework to show how experiments conducted at relatively high [$O_{3(g)}$] and [solute] can be translated to a range of atmospheric conditions (i.e. cloud droplets and aerosols).

V. Extension to Atmospheric Cloud Droplet and Aerosol Conditions

Here, we examine how the kinetic information obtained under laboratory conditions relate to those commonly found in the atmosphere by considering two contrasting cases: nitrite and MA. Shown in Fig. 10 are model predictions of γ over a broad range of droplet sizes and solute concentrations. The ozone reaction with MA is slow and occurs mainly in the bulk of the droplet,

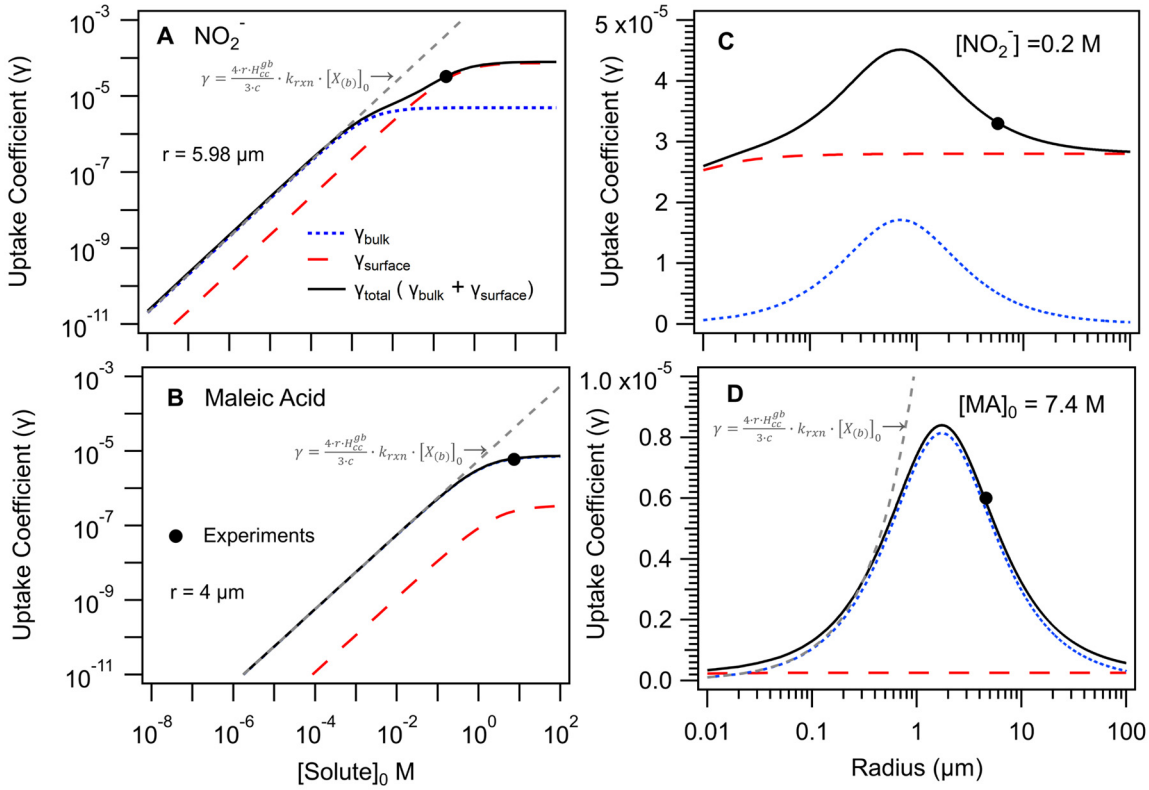

Figure 10: Predicted uptake coefficient vs. [solute]$_0$ for (A) NO_2^- (r = 5.98 μm) and (B) maleic acid (r = 4 μm). Predicted uptake coefficient vs. droplet radius for (C) NO_2^- and (D) maleic acid. Shown as dashed lines are predictions from 'dilute-limit' resistor model Eq. (30). Predicted uptake coefficients are shown with contributions from the bulk and surface reactions.

whereas the nitrite reaction is 200X faster with a large surface contribution. Shown in Fig 10A are predicted uptake coefficients for nitrite as a function of its concentration for a r = 5.98 μm droplet. At higher concentrations (0.1-1 M) the uptake coefficient is dominated by surface reactions. At micromolar concentrations, typical of fog and cloud droplets,[91] there is a shift from a surface-dominated to a bulk reaction mechanism. This is due to the decreasing quantity of NO_2^- at the interface, which depends, through the Langmuir equation, on $[NO_{2(b)}]$. Below 10^{-3} M the uptake coefficient approaches the limiting case where the droplet reactivity is well described by Eq. (30) ('dilute-limit' resistor case),[16] indicating that the reactive loss of O_3 is slower than its transport into the droplet. This is consistent with extrapolations to atmospheric conditions reported by Hunt *et al.*[50] As evident in Fig. 10A, there is a cross over region where $\gamma_s = \gamma_b$ indicating that surface and bulk reactions contribute equally to the total reactive uptake. For nitrite this occurs ~0.02 M and is easily computed using Eq. (36). This is a useful reference point to identify when resistor limiting cases can be reliably used or to predict when surface reactions in droplets might play a large role or can be safely neglected. For more strongly surface-active molecules (e.g., C_{10} diacids[73]), that undergo fast reactions with atmospheric trace gases, this cross over region extends into very dilute concentrations (Fig. S5), suggesting that surface reactions will dominate even under cloud water conditions.

The same set of predictions are made for maleic acid as shown in Fig. 10B and D. Unlike nitrite, MA is weakly surface active and reacts more slowing with O_3. The total uptake for the concentrations shown in Fig. 10 is controlled mainly by bulk reactions. At [MA] < 0.3 M the uptake coefficient is well described by Eq. (30) ('dilute-limit' resistor case)[16], indicating that the reactive loss of O_3 is slower than its transport into the droplet. At [MA] > 0.3 M, we observe the onset of transport limitations, as O_3 is consumed faster than it can be re-supplied by the gas phase.

This is the bulk depletion region where $[O_{3(b)}] < H_{cc}^{gb} \cdot [O_{3(g)}]$. Importantly this transport limited regime is commonly analyzed using Eq. (31) ('diffusion-limited' resistor limiting case)[16]. Although widely used, this resistor limiting case does not appear to make accurate predictions, likely because it does not account for the kinetic coupling of trace gas adsorption/desorption and solvation/desolvation with diffusion. Such coupling appears to be important[48] to describe multiphase chemistry in this transport limited regime.

Shown in Fig. 10C and 10D is the predicted size dependence of γ at a single solute concentration. For $[NO_{2(b)}^-]$ = 0.2 M, the surface reaction dominates and, as expected is independent of droplet size. The bulk contribution however, which does depend upon r, is non-negligible leading to a predicted size dependence of γ_{total} that is non-monotonic and peaks around ~700 nm. As described above, future experiments are needed to validate this prediction. For MA (Fig. 10D) the size dependence is dominated by γ_b with a maximum ~1.7 μm. At r > 1.7 μm, uptake decreases with size as transport timescales lengthen relative to reaction so that the overall reaction rate is controlled by the depleted $[O_{3(b)}]$ in the droplet. Below 1.7 μm transport of O_3 into the droplet is fast relative to its chemical loss such that $[O_{3(b)}] = H_{cc}^{gb} \cdot [O_{3(g)}]$, yielding an uptake dependence on size that is consistent with Eq. (30) ('dilute-limit' resistor case).

These two examples nicely illustrate that reactive uptake is an emergent phenomenon, which depends in complex ways on droplet size and reactant concentrations. For example, despite a common bimolecular rate coefficient for ozonolysis, laboratory experiments may be governed by surface reactions but then shift under atmospheric conditions towards a transformation governed entirely by aqueous phase chemistry occurring inside the droplet. Given that there are a broad range of particle sizes and solute concentrations (dilute cloud droplets vs. supersaturated

aerosols) found in our atmosphere, the equations presented here appear to be able to accurately predict the multiphase kinetics occurring under these vastly different conditions.

VI. Discussion and Implications

Here we present a new kinetic framework to explain trace gas (X) uptake and reaction. We validate predictions from this framework against five independent literature data sets. Our framework describes the Henry's Law constant as a product of two coupled equilibria linking trace gas adsorption/desorption at the interface with its solvation/desolvation in the bulk liquid. We describe solute (Y) partitioning to the surface with a third equilibrium and a Langmuir constant. The X+Y reaction, occurring at the interface, in the bulk, or in both locations, perturb these three coupled equilibria in complex ways, producing feedbacks and behavior that depend upon solute concentration and droplet size. Notably, we find that the behavior of these multiphase systems cannot be captured using simple resistor model limiting cases.

We derive a new expression to predict reactive uptake coefficients; explicitly accounting for surface and bulk reactions. This single expression,

$$\gamma_{total} = \gamma_s + \gamma_b = \frac{4 \cdot r \cdot [Y_{(b)}]}{3 \cdot \bar{c}} \cdot \left(\left[\frac{k_{s\_rxn} \cdot H_{cc}^{gs} \cdot \Gamma_{\infty}^{Y} \cdot K_{eq}^{Y}}{1 + K_{eq}^{Y} \cdot [Y_{(b)}]} \cdot \left(\frac{r^3 - (r-\delta)^3}{r^3} \right) \right] + \left[\frac{k_{b\_rxn} \cdot k_{transport} \cdot H_{cc}^{gb}}{k_{rxn}[Y_{(b)}] + k_{transport}} \right] \right) \quad \text{Eq. (44)}$$

can be used for predictions over a wide range of aerosol or droplet sizes and solute concentrations, from transport-limited reactive uptake in the bulk to surface-dominated reactions. This expression is particularly useful to predict how the multiphase kinetics, measured under laboratory conditions, can be reliably extrapolated to predict reaction rates in the atmosphere. While this framework was validated against experiment, there are some predictions and assumptions that require further experimental testing, such as the non-monotonic size dependence of γ for transport limited bulk reactions. Another assumption that requires testing is the approximation that the overall multiphase

transformation can be accurately described using only two kinetically active regions (gas/surface and surface/bulk), which neglects the formation of subsurface chemical gradients that extend into the droplet or aerosol interior.

The kinetics of X and Y are described by the following set of expressions,

$$\left[X_{(b)}\right]_t = \frac{k_{transport} \cdot H_{cc}^{gb} \cdot [X_{(g)}]}{k_{b\_rxn} \cdot \left[Y_{(b)}\right]_t + k_{transport}} \quad \text{Eq. (45)}$$

$$\left[Y_{(b)}\right]_t = \frac{k_{transport}}{k_{b\_rxn}} \cdot \boldsymbol{W}\left\{\frac{k_{b\_rxn} \cdot \left[Y_{(b)}\right]_0}{k_{transport}} \cdot exp\left(\frac{k_{b\_rxn} \cdot \left[Y_{(b)}\right]_0}{k_{transport}} - k_{b\_rxn} \cdot H_{cc}^{gb} \cdot \left[X_{(g)}\right] \cdot t\right)\right\} \quad \text{Eq. (46)}$$

$$[Y_{(s)}]_t = \frac{\boldsymbol{W}\left\{K_{eq}^{Y} \cdot \left[Y_{(b)}\right]_0 \cdot exp\left(K_{eq}^{Y} \cdot \left[Y_{(b)}\right]_0 - k_{s\_rxn} \cdot H_{cc}^{gs} \cdot [X_{(g)}] \cdot \Gamma_{\infty}^{Y} \cdot K_{eq}^{Y} \cdot \left(\frac{r^3 - (r-\delta)^3}{r^3}\right) \cdot t\right)\right\}}{K_{eq}^{Y}} \quad \text{Eq. (47)}$$

$$[Y_{(total\_s+b)}]_t = \frac{\boldsymbol{W}\left\{K_{eq}^{Y} \cdot \left[Y_{(b)}\right]_t \cdot exp\left(K_{eq}^{Y} \cdot \left[Y_{(b)}\right]_t - k_{s\_rxn} \cdot H_{cc}^{gs} \cdot [X_{(g)}] \cdot \Gamma_{\infty}^{Y} \cdot K_{eq}^{Y} \cdot \left(\frac{r^3 - (r-\delta)^3}{r^3}\right) \cdot t\right)\right\}}{K_{eq}^{Y}} \quad \text{Eq. (48)}$$

which are obtained by solving the integrated rate laws using Lambert **W** functions. Application of these expressions requires only a small number of quantities (e.g. $H_{cc}^{gb}, H_{cc}^{gs}, k_{rxn}, K_{eq}^{Y}, \Gamma_{\infty}^{Y}, D_x$) for X and Y to be known. These quantities can be obtained in MD simulations or simply measured using other experimental techniques.

The solute decay kinetics across five different experimental systems are well replicated using the Lambert function shown Eq. (48). The properties of these equations (and Lambert **W** functions in general) naturally yield a variety of functional forms for the kinetics (e.g. zero order vs. first order in [solute]) as has been previously observed in studies of enzyme-substrate binding kinetics.[79, 81, 82] Here, these different functional forms reflect changes in the multiphase reaction mechanism: surface vs. bulk dominated reactions, or kinetic vs. diffusional limited reactive uptake. Significant insight can therefore be gained by simply examining the decay kinetics. For example,

surface dominated reactions yield "exponential-like" kinetics (e.g. first order) as shown for nitrite, ascorbic acid and fumerate. The decay kinetics for transport limited bulk reactions (e.g., MA and AA) are zero order and appear linear in time. Under dilute solute conditions, dominated by bulk reactions, the decay kinetics shift from linear to exponential. In many previous studies, the functional form of the decay kinetics, interpreted under diffusion limited conditions (applying Eq 31), often yield a linear decay vs. time when plotted as the square-root of the normalized solute concentration. This kind of data analysis is often used to extract a bulk bimolecular rate coefficient for a reaction. Given the clear limitations of Eq. (31), as presented above, it appears that such a kinetic analysis, while simple, does not include key kinetic steps needed to accurately describe the multiphase transformation under diffusion-limited conditions.

While these equations account for a broad range of reaction conditions, they do not account for extremely fast reactions where $[X_{(ads)}]$ is depleted at the interface such that $\left[X_{(ads)}\right] < H_{cc}^{gs} \cdot \left[X_{(g)}\right]$. They also do not account for the case where the surface reaction consumes $Y_{(ads)}$ at rates that are faster than can be maintained through partitioning from the bulk. For ozonolysis, unlike OH reactions, these cases appear somewhat rare, with one notable exception. The reaction of ozone with aqueous iodide is ~1000x faster than the fastest reaction considered here and requires accounting for both trace gas and solute depletion at the interface, which will be addressed in a forthcoming publication.[86]

One central element of our model framework is the difference in solvation energy between gas phase and adsorbed X, which is needed to compute H_{cc}^{gs}. This information is readily available from MD simulations and has been used by a number of authors.[55, 92, 93] While there are many MD studies of pure water interfaces, there are comparably fewer studies examining how interface hydration energies of trace gases change in the presence of ions or other solutes. While it is well

documented that H_{cc}^{gb} decreases with ionic strength, it is less clear how ionic strength might impact solvation of a trace gas at an interface. To the extent that higher ionic strengths "salt out" trace gases, this could produce further enrichment of X at the interface, thus enhancing the importance of surface reactions. Lastly, fewer studies of interface solvation energies in organic solvents exist, which would be needed to apply these equations to understand multiphase transformations in purely organic aerosols.

The equations we present are derived from a model that explicitly accounts for the coupling of surface and bulk elementary steps and therefore avoids many of the assumptions inherent in resistor formulations of reactive uptake. These equations don't require making *a priori* assumptions about where the reaction occurs and/or under what limiting conditions. The framework provides a simple, yet physically realistic, way of connecting rate coefficients measured under dilute conditions in lab-scale reactors with the multiphase chemistry occurring in nanometer-sized aerosol and microdroplets present in our atmosphere.

Supplementary Material:

Tables S1- S4. Figures S1-S4

Acknowledgements: This work was supported by the Condensed Phase and Interfacial Molecular Science Program (CPIMS), in the Chemical Sciences Geosciences and Biosciences Division of the Office of Basic Energy Sciences of the U.S. Department of Energy under Contract No. DE-AC02-05CH11231. We are grateful to Professor Yuan-Pin Chang (National Sun Yat-sen University) for providing us the ascorbic acid kinetic data. We thank Dr. Meirong Zeng (LBNL) and Ryan Reynolds (LBNL and UC Berkeley) for helpful discussions.

References

1. J. P. D. Abbatt, A. K. Y. Lee and J. A. Thornton, Quantifying trace gas uptake to tropospheric aerosol: recent advances and remaining challenges, *Chem. Soc. Rev.*, 2012, **41**, 6555-6581.

2. C. E. Kolb, R. A. Cox, J. P. D. Abbatt, M. Ammann, E. J. Davis, D. J. Donaldson, B. C. Garrett, C. George, P. T. Griffiths, D. R. Hanson, M. Kulmala, G. McFiggans, U. Poschl, I. Riipinen, M. J. Rossi, Y. Rudich, P. E. Wagner, P. M. Winkler, D. R. Worsnop and C. D. O' Dowd, An overview of current issues in the uptake of atmospheric trace gases by aerosols and clouds, *Atmos. Chem. Phys.*, 2010, **10**, 10561-10605.

3. A. R. Ravishankara, Heterogeneous and Multiphase Chemistry in the Troposphere, *Science*, 1997, **276**, 1058-1065.

4. J. B. Burkholder, J. P. D. Abbatt, I. Barnes, J. M. Roberts, M. L. Melamed, M. Ammann, A. K. Bertram, C. D. Cappa, A. G. Carlton, L. J. Carpenter, J. N. Crowley, Y. Dubowski, C. George, D. E. Heard, H. Herrmann, F. N. Keutsch, J. H. Kroll, V. F. McNeill, N. L. Ng, S. A. Nizkorodov, J. J. Orlando, C. J. Percival, B. Picquet-Varrault, Y. Rudich, P. W. Seakins, J. D. Surratt, H. Tanimoto, J. A. Thornton, Z. Tong, G. S. Tyndall, A. Wahner, C. J. Weschler, K. R. Wilson and P. J. Ziemann, The Essential Role for Laboratory Studies in Atmospheric Chemistry, *Environ. Sci. Technol.*, 2017, **51**, 2519-2528.

5. T. Berkemeier, A. Mishra, C. Mattei, A. J. Huisman, U. K. Krieger and U. Pöschl, Ozonolysis of Oleic Acid Aerosol Revisited: Multiphase Chemical Kinetics and Reaction Mechanisms, *ACS Earth and Space Chemistry*, 2021, **5**, 3313-3323.

6. F. A. Houle, W. D. Hinsberg and K. R. Wilson, Oxidation of a model alkane aerosol by OH radical: the emergent nature of reactive uptake, *Phys. Chem. Chem. Phys.*, 2015, **17**, 4412-4423.

7. C. E. Kolb, R. A. Cox, J. P. D. Abbatt, M. Ammann, E. J. Davis, D. J. Donaldson, B. C. Garrett, C. George, P. T. Griffiths, D. R. Hanson, M. Kulmala, G. McFiggans, U. Pöschl, I. Riipinen, M. J. Rossi, Y. Rudich, P. E. Wagner, P. M. Winkler, D. R. Worsnop and C. D. O' Dowd, An overview of current issues in the uptake of atmospheric trace gases by aerosols and clouds, *Atmos. Chem. Phys.*, 2010, **10**, 10561-10605.

8. R. Sander, Modeling Atmospheric Chemistry: Interactions between Gas-Phase Species and Liquid Cloud/Aerosol Particles, *Surveys in Geophysics*, 1999, **20**, 1-31.

9. P. V. Danckwerts, *Gas-liquid reactions*, John Wiley & Sons, Ltd, 1971.

10. P. V. Danckwerts, Absorption by simultaneous diffusion and chemical reaction into particles of various shapes and into falling drops, *Transactions of the Faraday Society*, 1951, **47**, 1014-1023.

11. S. E. Schwartz, *Mass-Transport Considerations Pertinent to Aqueous Phase Reactions of Gases in Liquid-Water Clouds*, NATO ASI Series: Chemistry of Multiphase Atmospheric Systems, Springer Berlin Heidelberg, Berlin, Heidelberg, 1986.

12. B. Shi and J. H. Seinfeld, On mass transport limitation to the rate of reaction of gases in liquid droplets, *Atmos. Environ. Part A*, 1991, **25**, 2371-2383.

13. D. R. Hanson, A. R. Ravishankara and S. Solomon, Heterogeneous reactions in sulfuric acid aerosols: A framework for model calculations, *J. Geophys. Res.: Atmos.*, 1994, **99**, 3615-3629.

14. P. Davidovits, C. E. Kolb, L. R. Williams, J. T. Jayne and D. R. Worsnop, Mass accommodation and chemical reactions at gas-liquid interfaces, *Chem. Rev.*, 2006, **106**, 1323-1354.

15. G. M. Nathanson, P. Davidovits, D. R. Worsnop and C. E. Kolb, Dynamics and kinetics at the gas-liquid interface, *J. Phys. Chem.*, 1996, **100**, 13007-13020.

16. D. R. Worsnop, J. W. Morris, Q. Shi, P. Davidovits and C. E. Kolb, A chemical kinetic model for reactive transformations of aerosol particles, *Geophys. Res. Lett.*, 2002, **29**, 57-51-57-54.

17. D. R. Hanson, Surface-Specific Reactions on Liquids, *J. Phys. Chem. B*, 1997, **101**, 4998-5001.

18. J. T. Jayne, P. Davidovits, D. R. Worsnop, M. S. Zahniser and C. E. Kolb, Uptake of sulfur dioxide(G) by aqueous surfaces as a function of pH: the effect of chemical reaction at the interface, *J. Phys. Chem.*, 1990, **94**, 6041-6048.

19. U. Pöschl, Y. Rudich and M. Ammann, Kinetic model framework for aerosol and cloud surface chemistry and gas-particle interactions – Part 1: General equations, parameters, and terminology, *Atmos. Chem. Phys.*, 2007, **7**, 5989-6023.

20. M. Ammann, U. Pöschl and Y. Rudich, Effects of reversible adsorption and Langmuir–Hinshelwood surface reactions on gas uptake by atmospheric particles, *Phys. Chem. Chem. Phys.*, 2003, **5**, 351-356.

21. R. G. Remorov and C. George, Analysis of chemical kinetics at the gas-aqueous interface for submicron aerosols, *Phys. Chem. Chem. Phys.*, 2006, **8**, 4897-4901.

22. G. D. Smith, E. Woods, C. L. DeForest, T. Baer and R. E. Miller, Reactive Uptake of Ozone by Oleic Acid Aerosol Particles: Application of Single-Particle Mass Spectrometry to Heterogeneous Reaction Kinetics, *J. Phys. Chem. A*, 2002, **106**, 8085-8095.

23. C. G. Moreno, O. Gálvez, V. López-Arza Moreno, E. M. Espildora-García and M. T. Baeza-Romero, A revisit of the interaction of gaseous ozone with aqueous iodide. Estimating the contributions of the surface and bulk reactions, *Phys. Chem. Chem. Phys.*, 2018, **20**, 27571-27584.

24. J. Li and D. A. Knopf, Representation of Multiphase OH Oxidation of Amorphous Organic Aerosol for Tropospheric Conditions, *Environ. Sci. Technol.*, 2021, **55**, 7266-7275.

25. J. N. Crowley, M. Ammann, R. A. Cox, R. G. Hynes, M. E. Jenkin, A. Mellouki, M. J. Rossi, J. Troe and T. J. Wallington, Evaluated kinetic and photochemical data for atmospheric chemistry: Volume V – heterogeneous reactions on solid substrates, *Atmos. Chem. Phys.*, 2010, **10**, 9059-9223.

26. M. Ammann, R. A. Cox, J. N. Crowley, M. E. Jenkin, A. Mellouki, M. J. Rossi, J. Troe and T. J. Wallington, Evaluated kinetic and photochemical data for atmospheric chemistry: Volume VI – heterogeneous reactions with liquid substrates, *Atmos. Chem. Phys.*, 2013, **13**, 8045-8228.

27. M. Ammann and U. Pöschl, Kinetic model framework for aerosol and cloud surface chemistry and gas-particle interactions – Part 2: Exemplary practical applications and numerical simulations, *Atmos. Chem. Phys.*, 2007, **7**, 6025-6045.

28. A. A. Wiegel, K. R. Wilson, W. D. Hinsberg and F. A. Houle, Stochastic methods for aerosol chemistry: a compact molecular description of functionalization and fragmentation in the heterogeneous oxidation of squalane aerosol by OH radicals, *Phys. Chem. Chem. Phys.*, 2015, **17**, 4398-4411.

29. G. D. Smith, E. Woods, T. Baer and R. E. Miller, Aerosol Uptake Described by Numerical Solution of the Diffusion−Reaction Equations in the Particle, *J. Phys. Chem. A*, 2003, **107**, 9582-9587.

30. C. Moreno, M.-T. Baeza-Romero, M. Sanz, Ó. Gálvez, V. López Arza, J. C. Ianni and E. Espíldora, Iodide conversion to iodate in aqueous and solid aerosols exposed to ozone, *Phys. Chem. Chem. Phys.*, 2020, **22**, 5625-5637.

31. P. S. J. Lakey, C. M. A. Eichler, C. Wang, J. C. Little and M. Shiraiwa, Kinetic multi-layer model of film formation, growth, and chemistry (KM-FILM): Boundary layer processes, multi-layer adsorption, bulk diffusion, and heterogeneous reactions, *Indoor Air*, 2021, **31**, 2070-2083.

32. S. Ingram, G. Rovelli, Y.-C. Song, D. Topping, C. S. Dutcher, S. Liu, L. Nandy, M. Shiraiwa and J. P. Reid, Accurate Prediction of Organic Aerosol Evaporation Using Kinetic Multilayer Modeling and the Stokes–Einstein Equation, *J. Phys. Chem. A*, 2021, **125**, 3444-3456.

33. T. Berkemeier, A. J. Huisman, M. Ammann, M. Shiraiwa, T. Koop and U. Pöschl, Kinetic regimes and limiting cases of gas uptake and heterogeneous reactions in atmospheric aerosols and clouds: a general classification scheme, *Atmos. Chem. Phys.*, 2013, **13**, 6663-6686.

34. C. Pfrang, M. Shiraiwa and U. Pöschl, Coupling aerosol surface and bulk chemistry with a kinetic double layer model (K2-SUB): oxidation of oleic acid by ozone, *Atmos. Chem. Phys.*, 2010, **10**, 4537-4557.

35. M. Shiraiwa, C. Pfrang and U. Pöschl, Kinetic multi-layer model of aerosol surface and bulk chemistry (KM-SUB): the influence of interfacial transport and bulk diffusion on the oxidation of oleic acid by ozone, *Atmos. Chem. Phys.*, 2010, **10**, 3673-3691.

36. M. Shiraiwa, R. M. Garland and U. Pöschl, Kinetic double-layer model of aerosol surface chemistry and gas-particle interactions (K2-SURF): Degradation of polycyclic aromatic hydrocarbons exposed to O₃, NO₂, H₂O, OH and NO₃, *Atmos. Chem. Phys.*, 2009, **9**, 9571-9586.

37. M. Shiraiwa, C. Pfrang, T. Koop and U. Pöschl, Kinetic multi-layer model of gas-particle interactions in aerosols and clouds (KM-GAP): linking condensation, evaporation and chemical reactions of organics, oxidants and water, *Atmos. Chem. Phys.*, 2012, **12**, 2777-2794.

38. P. Roldin, A. C. Eriksson, E. Z. Nordin, E. Hermansson, D. Mogensen, A. Rusanen, M. Boy, E. Swietlicki, B. Svenningsson, A. Zelenyuk and J. Pagels, Modelling non-equilibrium secondary organic aerosol formation and evaporation with the aerosol dynamics, gas- and particle-phase chemistry kinetic multilayer model ADCHAM, *Atmos. Chem. Phys.*, 2014, **14**, 7953-7993.

39. T. Berkemeier, M. Ammann, U. K. Krieger, T. Peter, P. Spichtinger, U. Pöschl, M. Shiraiwa and A. J. Huisman, Technical note: Monte Carlo genetic algorithm (MCGA) for model analysis of multiphase chemical kinetics to determine transport and reaction rate coefficients using multiple experimental data sets, *Atmos. Chem. Phys.*, 2017, **17**, 8021-8029.

40. F. A. Houle, R. E. H. Miles, C. J. Pollak and J. P. Reid, A purely kinetic description of the evaporation of water droplets, *J. Chem. Phys.*, 2021, **154**, 054501.

41. K. R. Wilson, A. M. Prophet, G. Rovelli, M. D. Willis, R. J. Rapf and M. I. Jacobs, A kinetic description of how interfaces accelerate reactions in micro-compartments, *Chem. Sci.*, 2020, **11**, 8533-8545.

42. F. A. Houle, A. A. Wiegel and K. R. Wilson, Predicting Aerosol Reactivity Across Scales: from the Laboratory to the Atmosphere, *Environ. Sci. Technol.*, 2018, **52**, 13774-13781.

43. N. Heine, C. Arata, A. H. Goldstein, F. A. Houle and K. R. Wilson, Multiphase Mechanism for the Production of Sulfuric Acid from SO2 by Criegee Intermediates Formed During the Heterogeneous Reaction of Ozone with Squalene, *J. Phys. Chem. Lett.*, 2018, **9**, 3504-3510.

44. F. A. Houle, A. A. Wiegel and K. R. Wilson, Changes in Reactivity as Chemistry Becomes Confined to an Interface. The Case of Free Radical Oxidation of C30H62 Alkane by OH, *J. Phys. Chem. Lett.*, 2018, **9**, 1053-1057.

45. N. Heine, F. A. Houle and K. R. Wilson, Connecting the Elementary Reaction Pathways of Criegee Intermediates to the Chemical Erosion of Squalene Interfaces during Ozonolysis, *Environ. Sci. Technol.*, 2017, **51**, 13740-13748.

46. M. J. Liu, A. A. Wiegel, K. R. Wilson and F. A. Houle, Aerosol Fragmentation Driven by Coupling of Acid–Base and Free-Radical Chemistry in the Heterogeneous Oxidation of Aqueous Citric Acid by OH Radicals, *J. Phys. Chem. A*, 2017, **121**, 5856-5870.

47. A. A. Wiegel, M. J. Liu, W. D. Hinsberg, K. R. Wilson and F. A. Houle, Diffusive confinement of free radical intermediates in the OH radical oxidation of semisolid aerosols, *Phys. Chem. Chem. Phys.*, 2017, **19**, 6814-6830.

48. M. D. Willis and K. R. Wilson, Coupled surface and bulk kinetics govern the timescales of multiphase ozonolysis reactions, *ChemRxiv*, 2022, DOI: 10.26434/chemrxiv-2022-k2snf.

49. B. J. Dennis-Smither, F. H. Marshall, R. E. Miles, T. C. Preston and J. P. Reid, Volatility and oxidative aging of aqueous maleic acid aerosol droplets and the dependence on relative humidity, *J Phys Chem A*, 2014, **118**, 5680-5691.

50. O. R. Hunt, A. D. Ward and M. D. King, Heterogeneous oxidation of nitrite anion by gas-phase ozone in an aqueous droplet levitated by laser tweezers (optical trap): is there any evidence for enhanced surface reaction?, *Phys. Chem. Chem. Phys.*, 2015, **17**, 2734-2741.

51. M. Zeng and K. R. Wilson, Experimental evidence that halogen bonding catalyzes the heterogeneous chlorination of alkenes in submicron liquid droplets, *Chem. Sci.*, 2021, **12**, 10455-10466.

52. R. Vacha, P. Slavicek, M. Mucha, B. J. Finlayson-Pitts and P. Jungwirth, Adsorption of Atmospherically Relevant Gases at the Air/Water Interface: Free Energy Profiles of Aqueous Solvation of N2, O2, O3, OH, H2O, HO2, and H2O2, *J Phys Chem A*, 2004, **108**, 11573-11579.

53. J. Vieceli, M. Roeselova, N. Potter, L. X. Dang, B. C. Garrett and D. J. Tobias, Molecular Dynamics Simulations of Atmospheric Oxidants at the Air-Water Interface: Solvation and Accommodation of OH and O3, *J Phys Chem B*, 2005, **109**, 15876-15892.

54. J. M. Anglada, M. Martins-Costa, M. F. Ruiz-Lopez and J. S. Francisco, Spectroscopic signatures of ozone at the air-water interface and photochemistry implications, *Proc Natl Acad Sci U S A*, 2014, **111**, 11618-11623.

55. D. J. Donaldson and K. T. Valsaraj, Adsorption and Reaction of Trace Gas-Phase Organic Compounds on Atmospheric Water Film Surfaces: A Critical Review, *Environ. Sci. Technol.*, 2010, **44**, 865-873.

56. R. S. Taylor, D. Ray and B. C. Garrett, Understanding the Mechanism for the Mass Accommodation of Ethanol by a Water Droplet, *J. Phys. Chem. B*, 1997, **101**, 5473-5476.

57. W. Li, C. Y. Pak and Y.-L. S. Tse, Free energy study of H2O, N2O5, SO2, and O3 gas sorption by water droplets/slabs, *J. Chem. Phys.*, 2018, **148**, 164706.

58. Q. Shi, Y. Q. Li, P. Davidovits, J. T. Jayne, D. R. Worsnop, M. Mozurkewich and C. E. Kolb, Isotope Exchange for Gas-Phase Acetic Acid and Ethanol at Aqueous Interfaces: A Study of Surface Reactions, *J. Phys. Chem. B*, 1999, **103**, 2417-2430.

59. E. Stewart, R. L. Shields and R. S. Taylor, Molecular Dynamics Simulations of the Liquid/Vapor Interface of Aqueous Ethanol Solutions as a Function of Concentration, *J. Phys. Chem. B*, 2003, **107**, 2333-2343.

60. A. Morita and B. C. Garrett, Molecular theory of mass transfer kinetics and dynamics at gas–water interface, *Fluid Dyn. Res.*, 2008, **40**, 459-473.

61. M. A. Wilson and A. Pohorille, Adsorption and Solvation of Ethanol at the Water Liquid-Vapor Interface: A Molecular Dynamics Study, *J. Phys. Chem. B*, 1997, **101**, 3130-3135.

62. R. S. Taylor and B. C. Garrett, Accommodation of Alcohols by the Liquid/Vapor Interface of Water: Molecular Dynamics Study, *J. Phys. Chem. B*, 1999, **103**, 844-851.

63. B. C. Garrett, G. K. Schenter and A. Morita, Molecular Simulations of the Transport of Molecules across the Liquid/Vapor Interface of Water, *Chem. Rev.*, 2006, **106**, 1355-1374.

64. P. Davidovits, J. T. Jayne, S. X. Duan, D. R. Worsnop, M. S. Zahniser and C. E. Kolb, Uptake of gas molecules by liquids: a model, *J. Phys. Chem.*, 1991, **95**, 6337-6340.

65. C. J. H. Knox and L. F. Phillips, Capillary-Wave Model of Gas-Liquid Exchange, *J. Phys. Chem. B*, 1998, **102**, 8469-8472.

66. K. R. Wilson, A. M. Prophet, G. Rovelli, M. D. Willis, R. J. Rapf and M. I. Jacobs, A kinetic description of how interfaces accelerate reactions in micro-compartments, *Chem. Sci.*, 2020, DOI: 10.1039/d0sc03189e.

67. R. G. Remorov and M. W. Bardwell, Langmuir approach in the study of interface mass transfer, *Surf. Sci.*, 2005, **585**, 59-65.

68. I. Langmuir, The Adsorption of Gases on Plane Surfaces of Glass, Mica and Platinum, *J. Amer. Chem. Soc.*, 1918, **40**, 1361-1403.

69. Y.-P. Chang, S.-J. Wu, M.-S. Lin, C.-Y. Chiang and G. G. Huang, Ionic-strength and pH dependent reactivities of ascorbic acid toward ozone in aqueous micro-droplets studied using aerosol optical tweezers, *Phys. Chem. Chem. Phys.*, 2021, **23**, 10108-10117.

70. M. D. King, K. C. Thompson, A. D. Ward, C. Pfrang and B. R. Hughes, Oxidation of biogenic and water-soluble compounds in aqueous and organic aerosol droplets by ozone: a kinetic and product analysis approach using laser Raman tweezers, *Faraday Discuss.*, 2008, **137**, 173-192.

71. A. Einstein, Über die von der molekularkinetischen Theorie der Wärme geforderte Bewegung von in ruhenden Flüssigkeiten suspendierten Teilchen, *Annalen der Physik*, 1905, **322**, 549-560.

72. M. von Smoluchowski, Zur kinetischen Theorie der Brownschen Molekularbewegung und der Suspensionen, *Annalen der Physik*, 1906, **326**, 756-780.

73. G. Bleys and P. Joos, Adsorption kinetics of bolaform surfactants at the air/water interface, *J. Phys. Chem.*, 1985, **89**, 1027-1032.

74. F. Jin, R. Balasubramaniam and K. J. Stebe, Surfactant adsorption to spherical particles: the intrinsic length scale governing the shift from diffusion to kinetic-controlled mass transfer, *The Journal of Adhesion*, 2004, **80**, 773-796.

75. J. H. Lambert, Observations variae in mathesin puram., *Acta. Helv.*, 1758, **3**, 128-168.

76. R. M. Corless, G. H. Gonnet, D. E. G. Hare, D. J. Jeffrey and D. E. Knuth, On the LambertW function, *Advances in Computational Mathematics*, 1996, **5**, 329-359.

77. S. Schnell and C. Mendoza, Closed Form Solution for Time-dependent Enzyme Kinetics, *Journal of Theoretical Biology*, 1997, **187**, 207-212.

78. I. Kesisoglou, G. Singh and M. Nikolaou, The Lambert function should be in the engineering mathematical toolbox, *Computers & Chemical Engineering*, 2021, **148**, 107259.

79. B. W. Williams, The Utility of the Lambert Function W[a exp(a − bt)] in Chemical Kinetics, *Journal of Chemical Education*, 2010, **87**, 647-651.

80. D. Belkić, The Euler T and Lambert W functions in mechanistic radiobiological models with chemical kinetics for repair of irradiated cells, *Journal of Mathematical Chemistry*, 2018, **56**, 2133-2193.

81. C. T. Goudar, S. K. Harris, M. J. McInerney and J. M. Suflita, Progress curve analysis for enzyme and microbial kinetic reactions using explicit solutions based on the Lambert W function, *Journal of Microbiological Methods*, 2004, **59**, 317-326.

82. M. Goličnik, On the Lambert W function and its utility in biochemical kinetics, *Biochemical Engineering Journal*, 2012, **63**, 116-123.

83. *Wolfram Research, Inc., Mathematica*, Champaign, Illinois, Version 13.0.0 edn., 2021.

84. D. A. Barry, J. Y. Parlange, L. Li, H. Prommer, C. J. Cunningham and F. Stagnitti, Analytical approximations for real values of the Lambert W-function, *Mathematics and Computers in Simulation*, 2000, **53**, 95-103.

85. B. Wu, Y. Zhou, C. W. Lim and H. Zhong, Analytical approximations to the Lambert W function, *Applied Mathematical Modelling*, 2022, **104**, 114-121.

86. A. M. Prophet and K. R. Wilson, Ozonolysis of Aqueous Iodide at the Air-Water Interface studied by Single Microdroplet Mass Spectrometry, *to be submitted*, 2022.

87. N. K. Richards-Henderson, A. H. Goldstein and K. R. Wilson, Large Enhancement in the Heterogeneous Oxidation Rate of Organic Aerosols by Hydroxyl Radicals in the Presence of Nitric Oxide, *J. Phys. Chem. Lett.*, 2015, **6**, 4451-4455.

88. J. Hoigné and H. Bader, Rate constants of reactions of ozone with organic and inorganic compounds in water—II: Dissociating organic compounds, *Water Research*, 1983, **17**, 185-194.

89. D. Giamalva, D. F. Church and W. A. Pryor, A comparison of the rates of ozonation of biological antioxidants and oleate and linoleate esters, *Biochemical and Biophysical Research Communications*, 1985, **133**, 773-779.

90. J. R. Kanofsky and P. D. Sima, Reactive Absorption of Ozone by Aqueous Biomolecule Solutions: Implications for the Role of Sulfhydryl Compounds as Targets for Ozone, *Archives of Biochemistry and Biophysics*, 1995, **316**, 52-62.

91. G. Lammel and J. N. Cape, Nitrous acid and nitrite in the atmosphere, *Chem. Soc. Rev.*, 1996, **25**, 361-369.

92. A. Habartová, K. T. Valsaraj and M. Roeselová, Molecular Dynamics Simulations of Small Halogenated Organics at the Air–Water Interface: Implications in Water Treatment and Atmospheric Chemistry, *J. Phys. Chem. A*, 2013, **117**, 9205-9215.

93. K. T. Valsaraj, F. S. Ehrenhauser, A. A. Heath and M. Vaitilingom,in *Food, Energy, and Water*, ed. S. Ahuja, Elsevier, Boston, 2015, DOI: https://doi.org/10.1016/B978-0-12-800211-7.00003-X, pp. 93-112.